

CO₂ and hydrography acquired by Autonomous Surface Vehicles from the Atlantic Ocean to the Mediterranean Sea: data correction and validation

Riccardo Martellucci¹, Michele Giani¹, Elena Mauri¹, Laurent Coppola², Melf Paulsen³, Marine Fourier², Sara Pensieri⁴, Vanessa Cardin¹, Carlotta Denticò⁵, Roberto Bozzano⁴, Carolina Cantoni⁶, Anna Luchetta⁶, Alfredo Izquierdo⁷, Miguel Bruno⁷, and Ingunn Skjelvan⁸

¹National Institute of Oceanography and Applied Geophysics (OGS), Trieste, Italy

²Oceanography Laboratory of Villefranche (LOV), Villefranche, France

³GEOMAR Helmholtz Centre for Ocean Research Kiel, Kiel, Germany

⁴National Research Council - Institute for the study of Anthropic Impact and Sustainability in the Marine Environment (CNR-IAS), Genova, Italy

⁵Department of Environmental Sciences, Informatics and Statistics, Università Cà Foscari, Venice, Italy

⁶National Research Council-Institute of Marine Sciences (CNR-ISMAR), Trieste, Italy

⁷University of Cádiz (UCA), Spain

⁸NORCE Norwegian Research Centre, Bjerknes Centre for Climate Research. Bergen, Norway

Corresponding author: Riccardo Martellucci (rmartellucci@ogs.it)

Abstract. The ATL2MED demonstration experiment involved two autonomous surface vehicles from Saildrone Inc. (SD) which travelled a route from the eastern tropical North Atlantic to the Adriatic Sea between October 2019 and July 2020. This nine-month experiment in a transition zone between the temperate and tropical belts represents a major challenge for SD's operations. The sensors on board were exposed to varying degrees of degradation and biofouling depending on the geographical area and season, which led to a deterioration of the measurements. As a result, several maintenance measures were required during the mission.

We address the difficulty of correcting the data during a period of COVID-19 restrictions, which significantly reduced the number of discrete samples planned for SD salinity and dissolved oxygen validation. This article details alternative correction methods for salinity and dissolved oxygen. Due to the lack of *in situ* data, model products have been used to correct the salinity data acquired by the SDs, and then the resulting corrected salinity was validated with data from fixed ocean stations, gliders, and Argo floats. In addition, dissolved oxygen data acquired from SDs after correction using air oxygen measurements were tested and found to be coherent with the variation of oxygen concentrations expected from change in temperature and phytoplankton abundance (from chlorophyll-a). The correction methods are relevant and useful in situations where validation capabilities are lacking, which was the case during the ATL2MED demonstration experiment. In future experiments, more frequent *in situ* sampling would improve data qualification and validation.

1 Introduction

Automated observations contribute to a steadily increasing knowledge of the ocean and its role in the global climate system. For a long time, fixed ocean stations and research vessels formed the backbone of the monitoring network. In recent years, efforts have been made to improve the frequency of acquisition through technological developments (e.g., EU infrastructures ICOS, <https://www.icos-cp.eu/>; EMSO, <https://emso.eu/>; EuroArgo,

41 <https://www.euro-argo.eu>). Among other improvements, fixed ocean stations and ships of opportunity are
42 equipped with autonomous and accurate sensors for partial pressure of CO₂ ($p\text{CO}_2$) measurements in addition to
43 sensors for complementary measurements (*e.g.*, water temperature, salinity, dissolved oxygen, pH, nutrients,
44 fluorescence) needed to understand the dynamics and the effects of CO₂ fluxes on the carbon budget. Despite
45 efforts to do so, it remains difficult to obtain a comprehensive overview of CO₂ fluxes at regional and larger scales
46 due to sparse coverage by fixed observatories, low measurement frequency and limited systematic reference
47 measurements.

48 One way to address such observational gaps (Tanhua et al., 2019) is to develop and deploy Autonomous Surface
49 Vehicles (ASV) equipped with a suite of sensors, and capable of measuring CO₂ fluxes at the air-sea interface with
50 gas reference, high sampling frequency and real-time data transmission. ASV monitoring systems have the
51 potential to collect data from large ocean areas and at a frequency that resolves processes at multiple time scales.
52 Nevertheless, there are challenges with those surface monitoring systems, and one of the most important is the
53 biofouling, which can interfere with measurements of *e.g.*, conductivity, dissolved oxygen and especially
54 chlorophyll-a (Chl-a), and could ultimately render the sensors inoperable (*e.g.*, Delauney et al., 2010). Regular
55 maintenance counteracts biofouling or at least reduces the impact on measurements, but this is not always possible
56 due to long distance from shore or from the maintenance vessel. Therefore, the value of ASV data depends heavily
57 on quality control and quality assurance.

58 During the 9-month-long demonstration experiment ATL2MED, two wind-driven Saildrone ASV (SD;
59 Gentemann et al., 2020) manufactured by Saildrone Inc. (Alameda, CA, USA) were used to improve data coverage
60 and link CO₂ surface observations at fixed ocean stations on a larger scale from the eastern tropical North Atlantic
61 (ETNA) to the central Mediterranean Sea. SDs are prone to errors primarily due to sensor drift, which can be
62 caused by either biofouling or malfunctioning sensor parts. During the ATL2MED demonstration experiment,
63 problems were found with the data collected by several SD sensors, and severe biofouling occurred, as expected
64 in such a long-duration experiment.

65 Still, the use of SDs provided the opportunity to expand and link fixed CO₂ observations at the surface on a
66 larger scale, particularly during the COVID-19 pandemic when access to ocean platforms and ship visits were
67 restricted or even prohibited. Furthermore, the demonstration experiment allowed us to focus SD measurements
68 on different marine ecosystems in the Atlantic Ocean and the Mediterranean Sea, which made it possible to assess
69 the quality of measurements across a wide range of values. The experiment additionally evaluated the ability of
70 such ASV to provide data with sufficient quality to be relevant for the scientific community.

71 The objective of the present work is to evaluate and correct the data collected by the SDs in order to provide
72 a homogenised and comparable data set useful for the study of processes such as air-sea gas exchange in the
73 Atlantic Ocean and Mediterranean Sea. While this paper focuses on the methods, a follow up paper will focus on
74 biogeochemical processes occurring in the area.

75

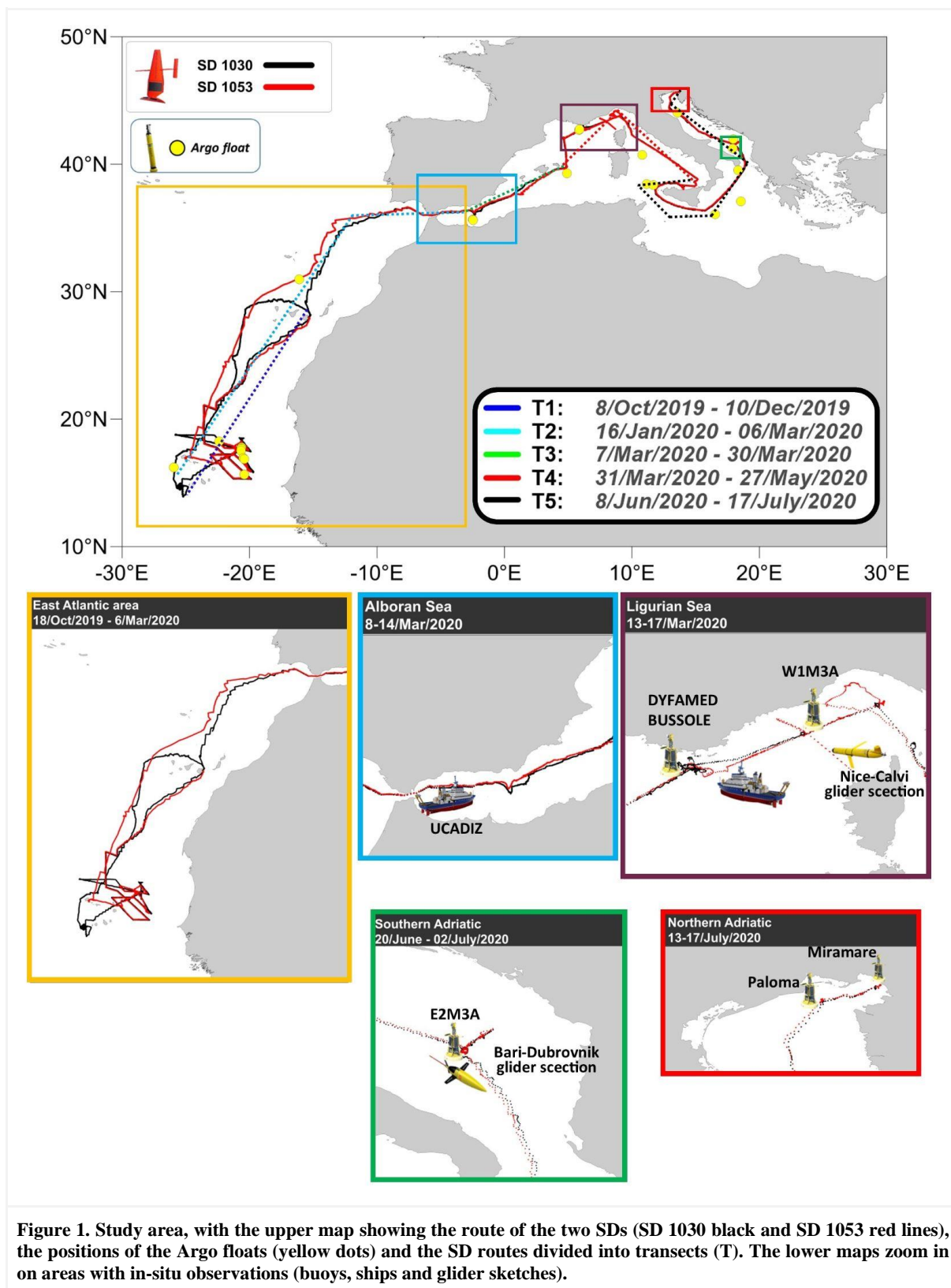
76 **2 Material**

77 **2.1 Data collection and experiment**

78 The ATL2MED demonstration experiment took place between 18 October 2019 and 17 July 2020 as a joint effort
79 among a number of European academic institutions and SD piloting team. A detailed description of the ATL2MED
80 demonstration experiment can be found in Skjelvan et al. (2021). During the experiment, the SDs crossed the
81 ETNA region, the Strait of Gibraltar, and the northern part of the western and central Mediterranean Sea including
82 the Ligurian Sea, the Strait of Sicily, the Strait of Otranto, and the Adriatic Sea (Fig. 1).

83 The aim of the ATL2MED demonstration experiment was to (1) study eddies in the Canary Current upwelling
84 system off West Africa jointly with a vessel-based research expedition (RV Meteor M160) and (2) to validate the
85 CO₂ measurements acquired at 5 fixed ocean stations (DYFAMED, W1M3A, E2M3A, PALOMA, and
86 MIRAMARE). Table 1 provides an overview of the various facilities and the times at which the SD visits were
87 carried out. A detailed description of the instruments and sensors installed on the different platforms as well as
88 their characteristics can be found in Tables S1, S2 and S3 of the Supplementary Material.

89



90

91 Maintenance operations ensured the reliability and accuracy of the data collected by the SDs. Throughout the
 92 expedition, the data collected by the SDs were categorised into different transects, designated as T1, T2, T3, T4,
 93 and T5. These transects corresponded to specific sections of the expedition timeline in terms of maintenance events
 94 (see Table S1 in Supplementary Material), which facilitates data correction.

95 The SDs were equipped with a number of autonomous sensors (CTD: conductivity, temperature, depth;
96 dissolved oxygen; fluorescence; pH; $p\text{CO}_2$; meteorological sensors). This study focuses primarily on sensors
97 acquiring temperature, salinity, dissolved oxygen, and $p\text{CO}_2$ data. This selection is based on the available options
98 for correcting the SD data sets: some of the sensors (*e.g.*, fluorescence) were so severely affected by biofouling
99 that it could not be accounted for, while others only worked for a short period of time (*e.g.*, Durafet Honeywell
100 pH sensor). One of the SDs (SD 1030) was equipped with an ASVCO₂ system developed by PMEL (NOAA's
101 Pacific Marine Environmental Laboratory). The ASVCO₂ system is a compressed version of the more voluminous
102 system described in detail in Sutton et al. (2014). Water from a depth of approximately 0.5 m is fed into a bubble
103 equilibrator (Friederich et al., 1995) and the partially dried $x\text{CO}_2$ is measured with an infrared detector (LI-COR
104 820 CO₂ gas analyser). A two points calibration was used where the first is a reference gas from NOAA/ERSL,
105 while the second is air purged for CO₂. An air inlet was mounted approximately 1 m above sea level and
106 atmospheric $x\text{CO}_2$ was measured between measurements of the sea surface. See Table S2 in the Supplementary
107 Material for the measurement frequency and initial accuracy of the SD sensors during the ATL2MED experiment.

108

109 2.2 Comparative datasets

110 2.2.1 Liguro-Provencal basin facilities

111 In the French EEZ, the open fixed station DYFAMED is located in the Ligurian Sea in the northwestern
112 Mediterranean Sea. The CNRS (French National Centre for Scientific Research) is in charge of the station as part
113 of the national MOOSE program (Coppola et al., 2019). At the DYFAMED site, a CARIOCA $p\text{CO}_2$ sensor ensures
114 autonomous measurements and detailed description can be found in Merlivat et al. (2018). In addition, gliders are
115 regularly operating the Nice-Calvi section where the DYFAMED site is located (MOOSE program; Coppola et
116 al., 2019; Bosse et al., 2015; Testor et al., 2019). During the demonstration experiment, a deployment of the
117 Slocum glider was used along the endurance line (MOOSE T00-43 mission) performed from 12 March to 20 June
118 2020. Table S2 includes information about which sensors the glider was equipped with. Discrete samples were
119 collected from the DYFAMED site in February and March 2020 for comparison with the $p\text{CO}_2$ sensor
120 measurements (Table S4).

121 The open fixed station W1M3A is located in the Italian EEZ of the Liguro-Provencal basin. Operated by
122 CNR-IAS, the W1M3A consists of a large spar buoy and a subsurface mooring positioned in the immediate
123 vicinity. A detailed description of the observatory can be found in Canepa et al. (2015) and some of this information
124 is found in Table S2. Discrete samples were collected from W1M3A in October 2020 (Table S4).

125

126 2.2.2 Adriatic Sea facilities

127 The fixed station E2M3A is situated in the open sea of the southern Adriatic Sea and is operated by OGS.
128 Information on this site is found in Bozzano et al. (2013) and Ravaioli et al. (2016). In the southern Adriatic, the
129 OGS also regularly operates an ocean glider at the Bari-Dubrovnik section (Mauri et al., 2016; Pirro et al., 2022;
130 Kokkini et al., 2019). During the AT2MED demonstration experiment, the glider transect was extended to include
131 the area of the E2M3A fixed station from 12 June to 2 July 2020. During the 20-day campaign 250 dives between
132 20 to 950 m profiles separated by 3-5 km and 4-6 hours were collected. Table S2 contains information about the
133 specific sensors mounted at the glider.

134 In the Gulf of Trieste in the northern Adriatic, the coastal stations PALOMA (operated by CNR-ISMAR) and
135 MIRAMARE (operated by OGS) are situated. Description of the PALOMA station is found in Ravaioli et al.
136 (2016) and Cantoni et al. (2012), while the MIRAMARE site is described in Ravaioli et al. (2016). See Table S2
137 for information about which sensors are used at the sites. By means of comparing the $p\text{CO}_2$ sensor measurements
138 performed at the sites, discrete carbon samples were collected near PALOMA on 15 July 2020 and in the vicinity
139 of MIRAMARE on 17 July 2020 (Table S4).

140

141 2.3 Shipboard data

142 Discrete samples for Dissolved Inorganic Carbon (DIC) and TA were collected onboard the RV Meteor (M160)
 143 during fall 2019 and analysed by GEOMAR. Discrete samples for DIC, TA, pH, and dissolved oxygen are
 144 regularly collected next to the fixed ocean stations, however, this was not always possible during the ATL2MED
 145 demonstration experiment due to COVID-19 pandemic restrictions. Table S4 gives an overview of the discrete
 146 samples collected during the ATL2MED demonstration experiment and their sampling depth and analysing
 147 methods.

148 In addition, salinity was measured continuously on board of the RV Ucadiz at a depth of 2.3 m between 5
 149 and 6 March 2020, when the SD crossed the Gibraltar Strait. Table S2 contains information about the sensor used.

150
 151 **Table 1. Research vessels and fixed ocean stations from which temperature, salinity and/or carbon measurements were**
 152 **compared with those of the SDs.**

Research vessel/ fixed station	Position	Institution	SD 1030	SD 1053
RV Meteor	17.80°N 20.60°W	GEOMAR (DE)	30 November 2019	12 December 2019
RV Ucadiz	36.55°N 6.31°W - 36.09°N 5.36°W	UCA (ES)	5-6 March 2020	5-6 March 2020
DYFAMED	43.42°N 7.87°E	CNRS (FR)	28 April 2020	23 April 2020
W1M3A*	43.83°N 9.12°E	CNR-IAS (IT)	29 April-2 May 2020	28 April-2 May 2020
E2M3A*	41.57°N 18.08°E	OGS (IT)	29 June-2 July 2020	29 June-23 July 2020
PALOMA*	45.62°N 13.57°E	CNR-ISMAR (IT)	15 July 2020	15 July 2020
MIRAMARE*	45.70°N 13.71°E	OGS (IT)	17 July 2020	17 July 2020

153 * These stations are part of the ICOS station network (Steinhoff et al., 2019).

154

155 2.4 Argo Float

156 Float data were retrieved from the Argo Coriolis Global Data Assembly Center in France (GDAC;
 157 <ftp://ftp.ifremer.fr/argo>, Wong et al., 2020). For each Argo float the variable SALINITY ADJUSTED was
 158 extracted, and then used for comparison with SD salinity data. Every profile close in space and time (1 day and 30
 159 km) was chosen and then salinity was averaged in the upper 5 m of the water column.

160

161 2.5 Model output

162 The Copernicus Marine Service (CMEMS) model product, specifically the Global Ocean 1/12° Physics Analysis
 163 and Forecast (<https://doi.org/10.48670/moi-00016>) and the Mediterranean Sea Physics Analysis and Forecast
 164 (Escudier et al., 2020, Clementi et al., 2021) were used. Daily data were developed for the global ocean and
 165 Mediterranean Sea.

166

167 2.6 Satellite product

168 To evaluate the ocean response, sea surface Chl-a (OCEANCOLOUR_MED_BGC_L3_NRT_009_141), sea
 169 surface temperature (Merchant et al., 2019, Buongiorno Nardelli et al., 2022) and the vertical structure of ocean

170 temperature (MEDSEA_MULTIYEAR_PHY_006_004) were downloaded from the CMEMS data portal and
171 analysed (Table S6 in the Supplementary Material).

172

173 3 Methods

174 3.1 Salinity

175 Here, the salinity is measured using the PSS-78 scale. During the first transect, T1 (Fig. 2), the two salinity sensors
176 on board the SDs showed high consistency (Fig. 2a, b). After the first maintenance in T2, the SD 1053 showed a
177 reduction in salinity of about 1 compared to the salinity measured by the SD 1030. In T3, the difference in salinity
178 decreased on average to 0.15. During this period, the SDs crossed the Alboran Sea characterised by high
179 thermohaline variability due to the presence of Atlantic and Mediterranean waters (Poulain et al., 2021), and the
180 high spatial and temporal variability in salinity distribution in the area (Capó et al., 2021) complicates the
181 understanding of the observed differences (i.e., sensor error or natural variability). In T4 and T5, salinity shifts of
182 1 were observed until the end of the experiment.

183 Given the large variability found in the salinity data of the SDs, a comparison with *in situ* data along the
184 trajectory of the experiment was necessary. We first identified the observing systems (fixed buoy, Argo float)
185 temporally and spatially close to the positions of the SDs. Salinity data, with a temporal and spatial interval lower
186 than 1 day and 30 km, respectively, were used for the comparison and/or correlation, however they were extremely
187 scarce.

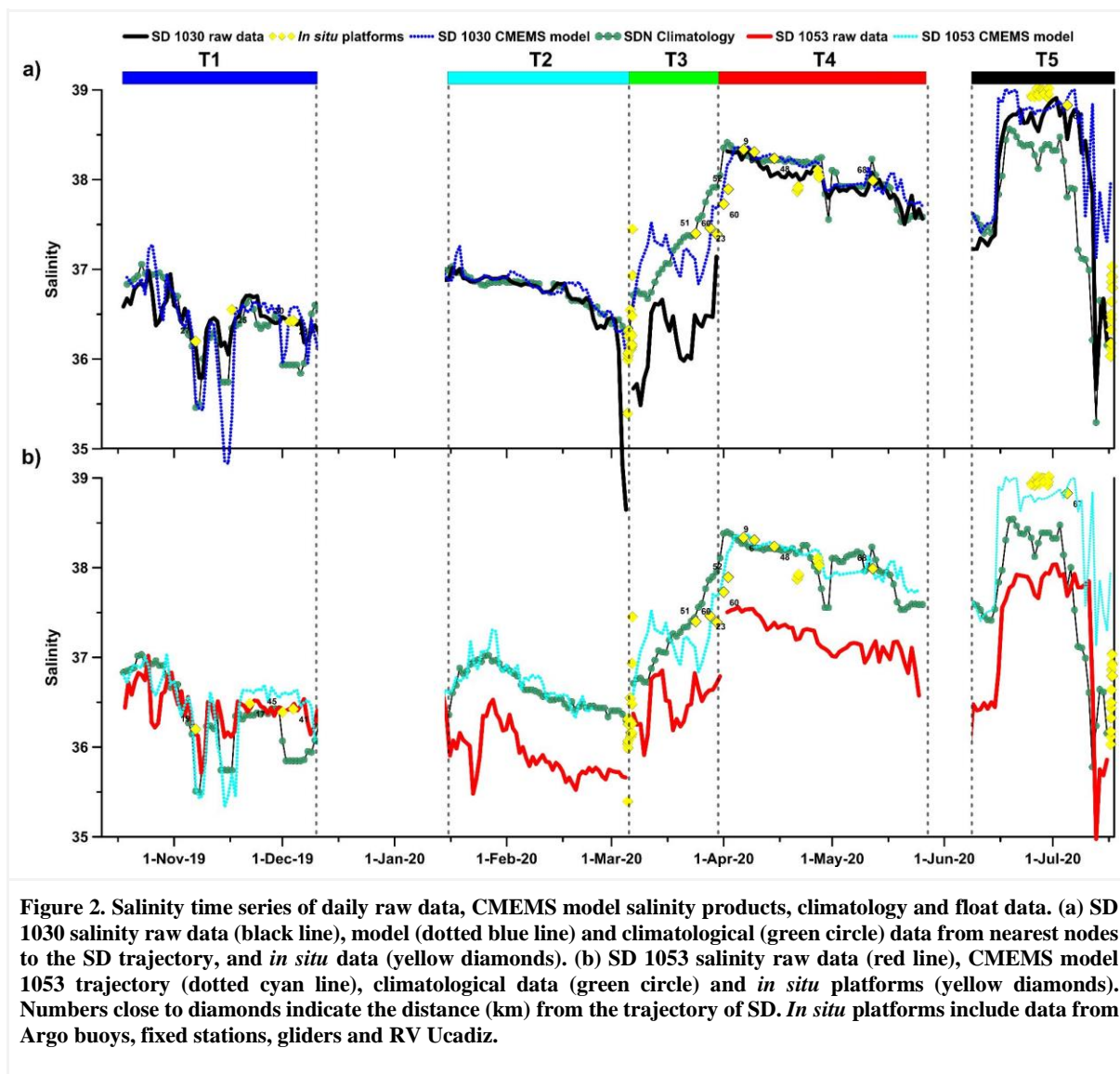
188 To further evaluate the salinity data of the two SDs, a comparison was made with climatological data,
189 considering the closest point in the climatology dataset to the SDs measurements (Fig. 2). SD 1030 exhibited
190 consistent salinity data in periods T1, T2, and T4 ($\Delta S < 0.1$), with deviations observed in periods T3 and T5 (Fig.
191 2a). Conversely, SD 1053 displayed consistent salinity data only in period T1 ($\Delta S < 0.1$), with higher deviations in
192 periods T2, T3, T4, and T5. Subsequent evaluation of the data distribution characteristics revealed variances
193 between the two SDs (Fig. 2b).

194 In T5, the climatology failed to represent salinity in Ionian and Adriatic Sea, characterised by a continuous
195 increase in salinity since 2017 (Mauri et al., 2021; Mhianovic et al., 2021; Menna et al., 2022; Neri et al., 2023;
196 Pranic et al., 2023). This was due to the bipolar behaviour of the Ionian Sea, subject to an alternation between the
197 highly saline waters of the Levantine Basin and the less saline waters of Atlantic origin (Pinardi et al., 2019; Gacic
198 et al., 2021; Menna et al., 2022; Civitarese et al., 2023).

199 To overcome the problem of lack of data, we decided to compare the data acquired by the SDs with the
200 reanalysis model products along the entire route (Fig. 2a, b). The model, while not deviating much from the *in situ*
201 and climatological data (Fig. 2), can provide salinity products along the SD's trajectory allowing to correct the
202 salinity recorded by the SD. Moreover, comparative works between the physical model and experimental
203 observations have shown a satisfactory correlation both in the open ocean (Escudier et al., 2021; Menna et al.,
204 2023) and in the coastal environment (Martellucci et al., 2021). Despite any limitations a model may have in such
205 cases, the use of model products allows a minimum spatial and temporal distance in the comparison of the along
206 track SD measurements. The nearest nodes (in km) with respect to the model data grid to the SD trajectory were
207 chosen. The salinity provided by the model along the two SD trajectories shows very similar values to that
208 measured by SD 1030 (Fig. 3). Salinity differences between the CMEMS model and the SD 1030 observations
209 show a difference less than 0.1 in T1, T2, T4 and T5. During the Alboran Sea crossing (T3), the observed salinity
210 deviated strongly from the model (about 0.6) over only 20 days. In contrast, SD 1053 showed deviating values
211 compared to the model and SD 1030, which cannot be explained by space-time variability. With the exception of
212 T1, the remaining transects (Fig. 3i-j) showed large deviations between model and observed salinities (T2: 0.8,
213 T3: 0.7, T4: 0.9, and T5: 1). This could be related to the long time between the SD 1053 maintenance (early January
214 and early May 2020), but it is more likely that a sensor error occurred in mid-January which even maintenance
215 could not correct.

216 The salinity correction was performed using a linear regression method in which the salinity data recorded by
217 the autonomous vehicles averaged over the day, were calibrated with the corresponding data from numerical
218 models. A strict criterion, with a significance level of $p < 0.05$ (Table 2), was applied to the correction process.

219



220

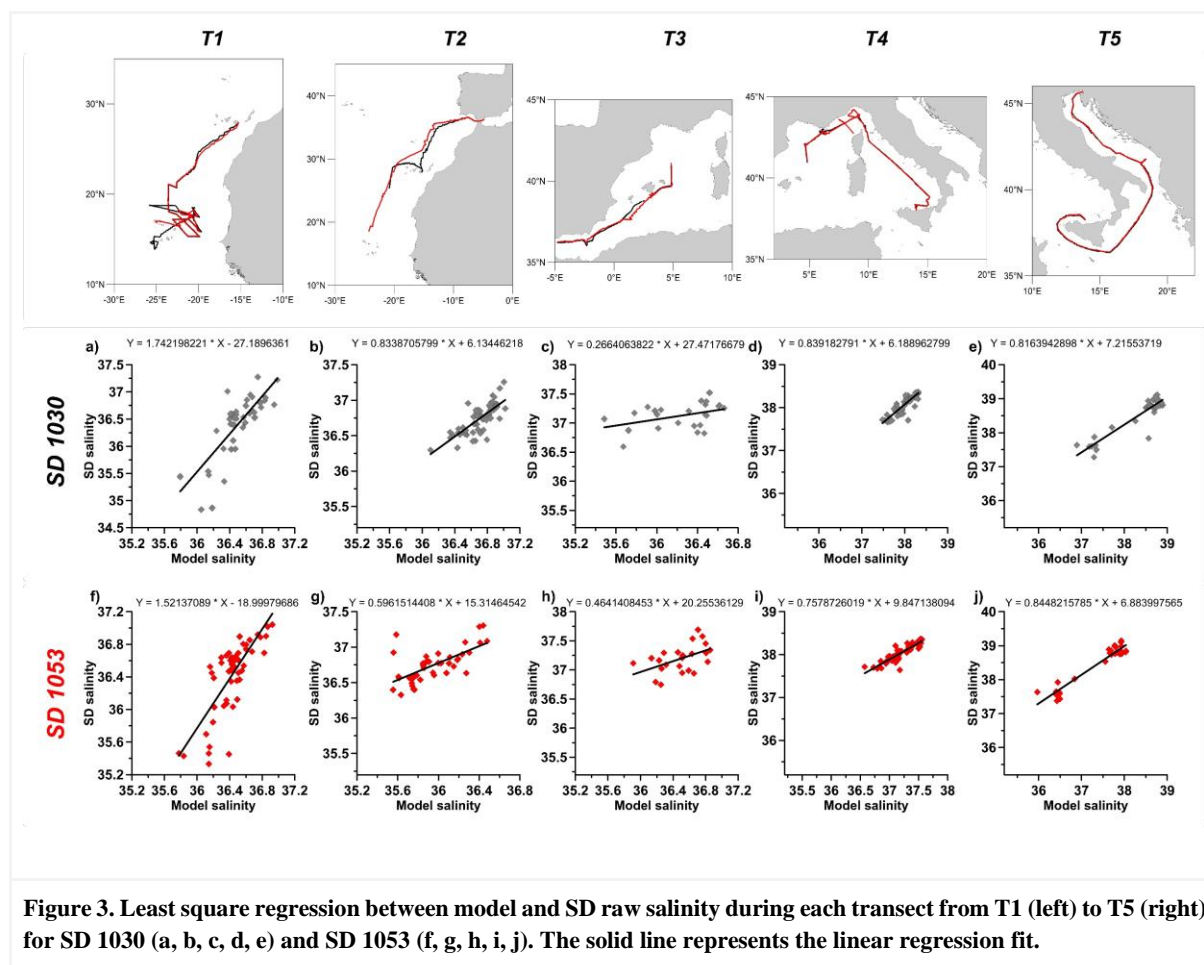
221 Table 2. Statistics for the salinity correction. T1, to T5 refer to the different transects, pval is the significance level,
 222 distribution refers to normal or non normal data distribution, R^2 is the correlation coefficient, RMSE is the root mean
 223 square error, and NaN refers to lack of data.

		Direct comparison				
		<i>T1</i>	<i>T2</i>	<i>T3</i>	<i>T4</i>	<i>T5</i>
SD 1030	<i>pval</i>	0.0007	0.04	<0.001	0.04	0.025
	<i>distribution</i>	non normal	non normal	normal	non normal	normal
	<i>R2</i>	0.59	0.61	0.19	0.71	0.85
	<i>RMSE</i>	-	-	0.9058	-	0.2789

SD 1053	<i>pval</i>	0.026	0.003	0.004	<0.001	<0.001
	<i>distribution</i>	non normal	normal	normal	normal	normal
	<i>R2</i>	0.08	0.44	0.25	0.789	0.919
	<i>RMSE</i>	-	0.826	0.7072	0.8444	1.1275

224

225

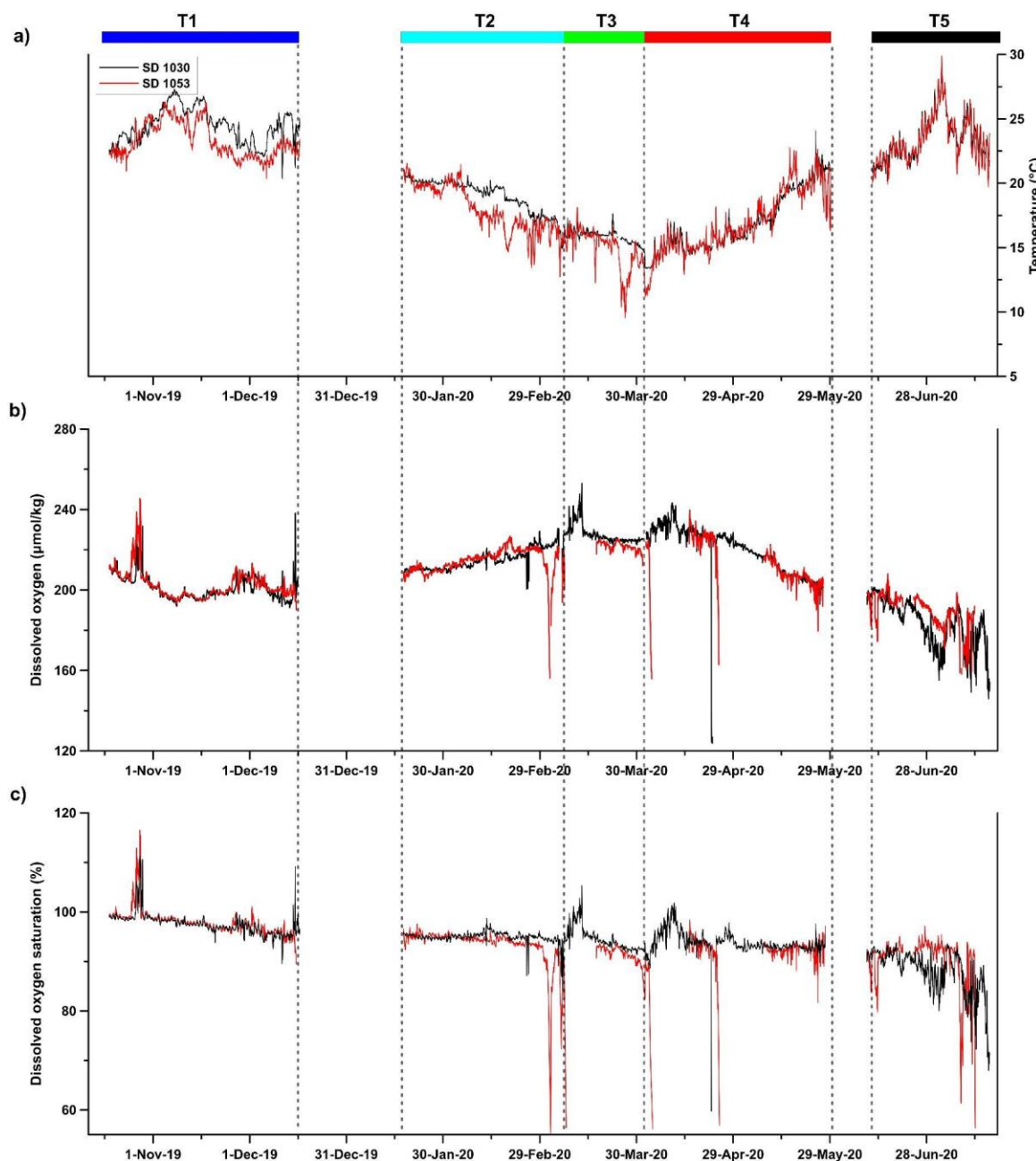


226

227 3.2 Dissolved Oxygen

228 Due to the strong dependence of dissolved oxygen on temperature, we first analyse the temperature along the track
 229 of the SDs. During the demonstration experiment, sea temperature (Fig. 4a) showed a seasonal signal similar to
 230 those observed at these latitudes (Pastor et al., 2019). The high observed temperature variability also includes the
 231 wide geographical coverage of the SDs. The highest temperatures were measured in November 2019 and July
 232 2020 in the tropical Atlantic and the southern Adriatic, respectively. The lowest temperatures were measured in
 233 the Gulf of Lion in April 2020. Along the SD tracks, the salinity (Fig. 2b) showed a gradual increase from the
 234 Atlantic Ocean to the eastern Mediterranean Sea. Given the correct temperature measurement, any dissolved
 235 oxygen drift can be assessed through comparison with dissolved oxygen saturation values. This procedure was

236 also used to correct Argo float data with climatological observations (Takeshita et al., 2013). The dissolved oxygen
 237 saturation showed a gradual decrease from 100% at the start of the demonstration experiment to 80% at the end
 238 (Fig. 4c). This behaviour is also reflected in the dissolved oxygen concentration, which decreases by about 40
 239 $\mu\text{mol/kg}$ for SD 1030 and 60 $\mu\text{mol/kg}$ for SD 1053 (Fig. 4b) over the course of nine months with standard deviation
 240 of the uncorrected oxygen record of 16 $\mu\text{mol/kg}$ and 72 $\mu\text{mol/kg}$ for SDs 1030 and 1053, respectively.
 241



242
 243
 244 **Figure 4. (a) Temperature, (b) dissolved oxygen concentration, and (c) dissolved oxygen saturation for the SD raw data**
 245 **(SD 1030 black line and SD 1053 red line).**
 246

247 Prior to applying correction all the outliers were excluded. After the first analysis we proceeded to correct the
 248 dissolved oxygen data, using the same oxygen correction method as used in the Argo program (Bittig et al., 2018).
 249 The principle of this method is to compare the dissolved oxygen measurements performed while the Argo oxygen
 250 sensor is in air with the oxygen partial pressure ($p\text{O}_2$) in air (Johnson et al., 2015). The latter variable is easily
 251 calculated from air temperature, air pressure, and relative humidity acquired by the SDs. Considering that the SD
 252 oxygen sensor is installed on the hull about 0.5 m below sea surface and that the SDs sailing cause mixing of the

253 water surface while sailing, we assume that the SDs oxygen sensors were in equilibrium with the atmosphere
 254 above, and furthermore, we can correct for the oxygen sensor drift using the in air calibration method (Bittig et al.,
 255 2018; Johnson et al., 2015). Specifically, we computed vapour pressure (V_p , in hPa) from the empirical equation
 256 reported in the operating manual of Aanderaa oxygen optode (model 4330) using the air temperature (T_{sd}) recorded
 257 from SDs:

$$258 \quad V_p = e^{(52.57 - \frac{6690.90}{T_{sd} + 273.15}) - 4.681 \cdot \ln T_{sd} + 273.15} \quad (1)$$

259 and expected partial pressure (E_{pp} , in hPa) from volume fraction of oxygen ($V_{fO_2}=0.20946$; Glueckauf, 1951),
 260 atmospheric pressure (AP_{sd}), vapour pressure (V_p) and relative humidity (RH_{sd}), as follows:

$$261 \quad E_{pp} = V_{fO_2} * (AP_{sd} - (V_p * \frac{RH_{sd}}{100})) \quad (2)$$

262 The E_{pp} was then compared to the pO_2 from the SDs to compute the gain factor (G) for daily correction.

$$263 \quad G = \frac{E_{pp}}{pO_{2sd}} \quad (3)$$

264 The corrected oxygen concentration (O_{2csd}) from the SDs was calculated from adjusting the oxygen data from SDs
 265 (O_{2sd}) with the gain factor.

$$266 \quad O_{2csd} = G * O_{2sd} \quad (4)$$

267 For each transect the mean gain was calculated and then, the gain factor was multiplied by the hourly oxygen
 268 data allowing to correct the time series.
 269

270 **3.3 Correction and adjustment of pCO_2 data**

271 **3.3.1 Fixed-sites pCO_2 data acquisition and qualification**

272 The pCO_2 measurements from the different fixed ocean stations were regularly compared to the pCO_2 calculated
 273 from discrete water samples collected by the fixed stations and analysed for TA, pH, and DIC. During the last half
 274 of the ATL2MED demonstration experiment, this routine was hampered due to COVID-19 restrictions, thus,
 275 between March and July 2020, there were less discrete carbon samples for comparison with fixed station pCO_2 .
 276 Furthermore, there was minor variability in sampling frequency with regards to the fixed station pCO_2
 277 measurements and in the pair of measured variables used for pCO_2 calculation (TA-pH or DIC-TA) between the
 278 different fixed ocean stations (see Table S2 and S4). During the ATL2MED demonstration experiment, DIC, TA,
 279 and pH were analysed according to SOP 2, 3b, and 6b, respectively (Dickson et al., 2007) with some minor local
 280 variations (Table S4). Certified Reference Material (CRM) and TRIS provided by Prof. A. Dickson (Scripps,
 281 USDC, USA) were used to determine the accuracy. pCO_2 was calculated using the speciation software CO2SYS
 282 (Pelletier et al., 2007), with the discrete carbon pairs TA-pH or DIC-TA as input variables. In the computation, the
 283 carbonate system constants from Lueker et al. (2000), the HSO_4^- constant from Dickson (1990), the total borate-
 284 salinity relationship of Lee et al. (2010), and the hydrogen fluoride constant K_F from Perez and Fraga (1987) were
 285 used. The uncertainties connected to this calculation ranged from 1.82% when using TA-pH as input variables to
 286 2.65% when DIC-TA were the input variables (Orr et al., 2018). Based on this, no adjustments were performed
 287 for the fixed station pCO_2 data when the deviation from pCO_2 calculated from discrete carbon data were less than
 288 $7.5 \mu atm$ and $10 \mu atm$ for the discrete carbon pairs TA-pH and DIC-TA, respectively. Uncertainty thresholds were
 289 set based on measurement uncertainties at each facility and temperature and pCO_2 in the vicinity of the fixed
 290 stations.
 291

292 3.3.2 Correction of SD CO₂ data

293 The general accuracy of the ASVCO₂ system attached to the SD 1030 was checked by PMEL prior to deployment
 294 by comparing the results with ESRL CO₂ standards traceable to WMO standards (Sutton et al., 2014). For this test,
 295 typically 6 standard gases were used. On the return of the ASVCO₂ system to PMEL, it was discovered that the
 296 span gas was adjusted too low to completely flush the detector and that this had been so during the whole
 297 ATL2MED demonstration experiment. Thus, the LI-COR had to be recalibrated at the PMEL lab and this implied
 298 that the onboard gas spanning was bypassed and new calibration coefficients were developed. Furthermore, the
 299 pre-mission test data from the PMEL lab were reprocessed using the new calibration coefficients. Based on the
 300 reported issues with the ASVCO₂ instrument, the accuracy of the CO₂ measurements is estimated to be < 5 µatm.
 301

302 4 Results and discussion

303 4.1 Salinity

304

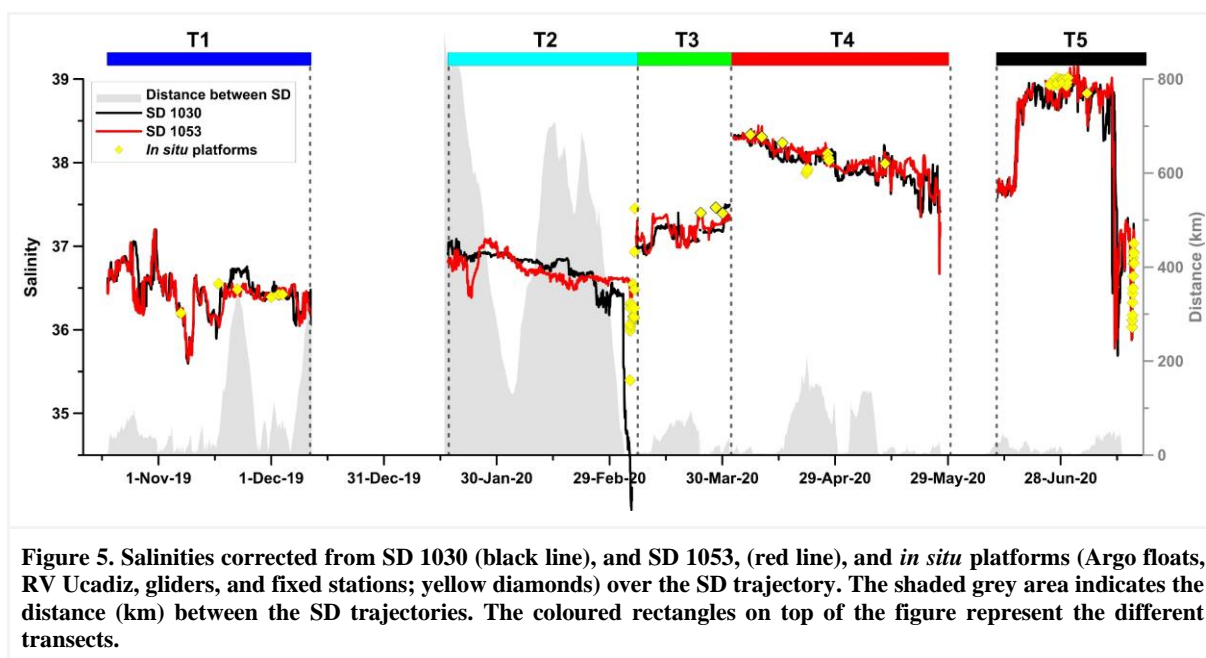


Figure 5. Salinities corrected from SD 1030 (black line), and SD 1053, (red line), and *in situ* platforms (Argo floats, RV Ucadiz, gliders, and fixed stations; yellow diamonds) over the SD trajectory. The shaded grey area indicates the distance (km) between the SD trajectories. The coloured rectangles on top of the figure represent the different transects.

305

306 The salinity correction were based on the significant linear correlation (Fig. 3) observed across the different
 307 periods (Table 2). The periods characterised by small differences in salinity (<0.1) were not corrected. In general,
 308 the corrected salinity for both SDs showed similar values (Fig. 5), and the major differences between the two SDs
 309 were mainly due to their temporal and spatial distance. Overall, the correction was largest for SD 1053 (see RMSE
 310 values in Table 2). To validate the salinity corrected data a comparison with different observing systems was done.

311 For SD1030, the corrected salinity data showed a slight overestimation of salinity, while the raw salinity data
 312 showed an underestimation. The SD 1030 salinity highlights good agreement in T1 with respect to the SD 1053
 313 (Fig. 5), the average difference was less than 0.05, the highest difference between Argo float data and corrected
 314 salinity data observed on 17 November 2019 was ~0.15. In T2, the comparison can only be made for SD 1030
 315 with only one Argo float profile.

316 Between T2 and T3 a drop in salinity was observed when the SDs crossed the ETNA area, where the salinity
 317 exhibits a strong variability (Reverdin et al., 2007), triggered by freshwater flux and eddy transport (Gordon and
 318 Giulivi, 2014). This salinity drop was also observed in the climatological data (Fig. 2).

319 The salinity in T2 (SD 1030) only slightly differed ($\Delta S \sim 0.05$) with respect to the model and values were in
 320 agreement with the observations of the Argo floats during the crossing of the Gibraltar strait. In T3 a significant
 321 difference was observed between model and observation (RMSE = 0.906; Table 2), while T4 was in line with the
 322 climatology as well as the fixed stations. In T5, the RMSE was 0.279 (Table 2), in the southern Adriatic, the SDs

323 spent four days sampling the area, which allowed a robust comparison between data from the E2M3A fixed ocean
324 station and the glider measurements. The comparison showed a very good agreement between the observations,
325 which had almost the same salinity. In the northern Adriatic (T5), the comparison with *in situ* data showed the
326 highest differences with respect to the other *in situ* platforms comparison. However, the comparison with the fixed
327 stations (MIRAMARE and PALOMA) showed the same temporal changes with an average difference between
328 the SDs and the MIRAMARE fixed ocean station of ~ 0.3 .

329 Regarding SD 1053, the comparison with the different fixed ocean stations shows that the corrected salinity
330 in T2, T3, T4 and T5 are consistent with the values measured at the stations (Argo float, glider, buoy, and RV
331 Ucadiz), the differences being mainly due to the distance between the different observatories and to the natural
332 variability of the areas. Also the corrected data fit well with climatological values and *in situ* platforms.
333 Considering that during T1 the SDs raw data showed a smaller deviation from the Argo float data, the salinity
334 correction was applied after this transect (*i.e.*, from the start of T2).

335 4.2 Dissolved oxygen

336 For dissolved oxygen concentration, it would have been preferable to be able to compare the SD data to discrete
337 data. However, over the period of the ATL2MED demonstration experiment, no discrete dissolved oxygen
338 measurements were available due to COVID-19 restrictions. The corrected oxygen measurements (Fig. 6a)
339 spanned from $170 \mu\text{mol/kg}$ to $270 \mu\text{mol/kg}$ highlighting the highest concentrations during spring 2020. Time series
340 of percent dissolved oxygen saturation did not show any significant trend (Fig. 6b). Oversaturation was observed
341 at the end of October 2019 ($\sim 115\%$) and at the beginning of March 2020 ($\sim 105\%$), while strong undersaturation
342 was observed at 1-2 of April 2020 ($\sim 95\%$) and 8-11 July 2020 ($\sim 92\%$).

343 Furthermore, we evaluated the change in dissolved oxygen measured by the two SDs in two different
344 geographical areas (the Canary Islands area and the Balearic basin), where dissolved oxygen showed
345 oversaturation (Fig. 7) and undersaturation (Fig. 8). In the first region, we made use of Chl-a data and temperature,
346 while in the second region, temperature was used to evaluate the representativeness of the correction with respect
347 to ecosystem dynamics. The optical sensors on the SDs and thus, the Chl-a measurements, were strongly affected
348 by biofouling for most of the demonstration experiment, which is why we do not use these measurements in this
349 work. However, during the 10 first days in October 2019, the Chl-a data acquired by the SDs seemed to produce
350 reasonable values in accordance to Delory et al. (2018), who found that for new sensors the increase in biofouling
351 needs weeks to become significant. We refer to these Chl-a data, collected by the SDs in the transect T1, when
352 explaining the dissolved oxygen oversaturation episode off the Canary Islands.

353 The oxygen saturation concentration can be expressed as a function of salinity and temperature, in terms of
354 solubility (Garcia and Gordon, 1992). The gas concentration in seawater depends on thermohaline characteristics
355 and biological activity. The solubility of oxygen decreases with increases in temperature and salinity, showing a
356 strong linear correlation. In the ocean, dissolved oxygen saturation slightly lower than 100% can be observed
357 during the cold seasons while in the warm season oxygen saturation is slightly higher than 100%, inversely to the
358 dissolved oxygen concentrations (*i.e.*, high concentrations during cold season and low in the warm season). This
359 is because heating and cooling are generally faster than outgassing, except for episodes of high wind speeds which
360 intensifies the air-sea gas exchange (Ulses et al., 2021). Furthermore, dissolved oxygen concentration is affected
361 by primary production and respiration.

362

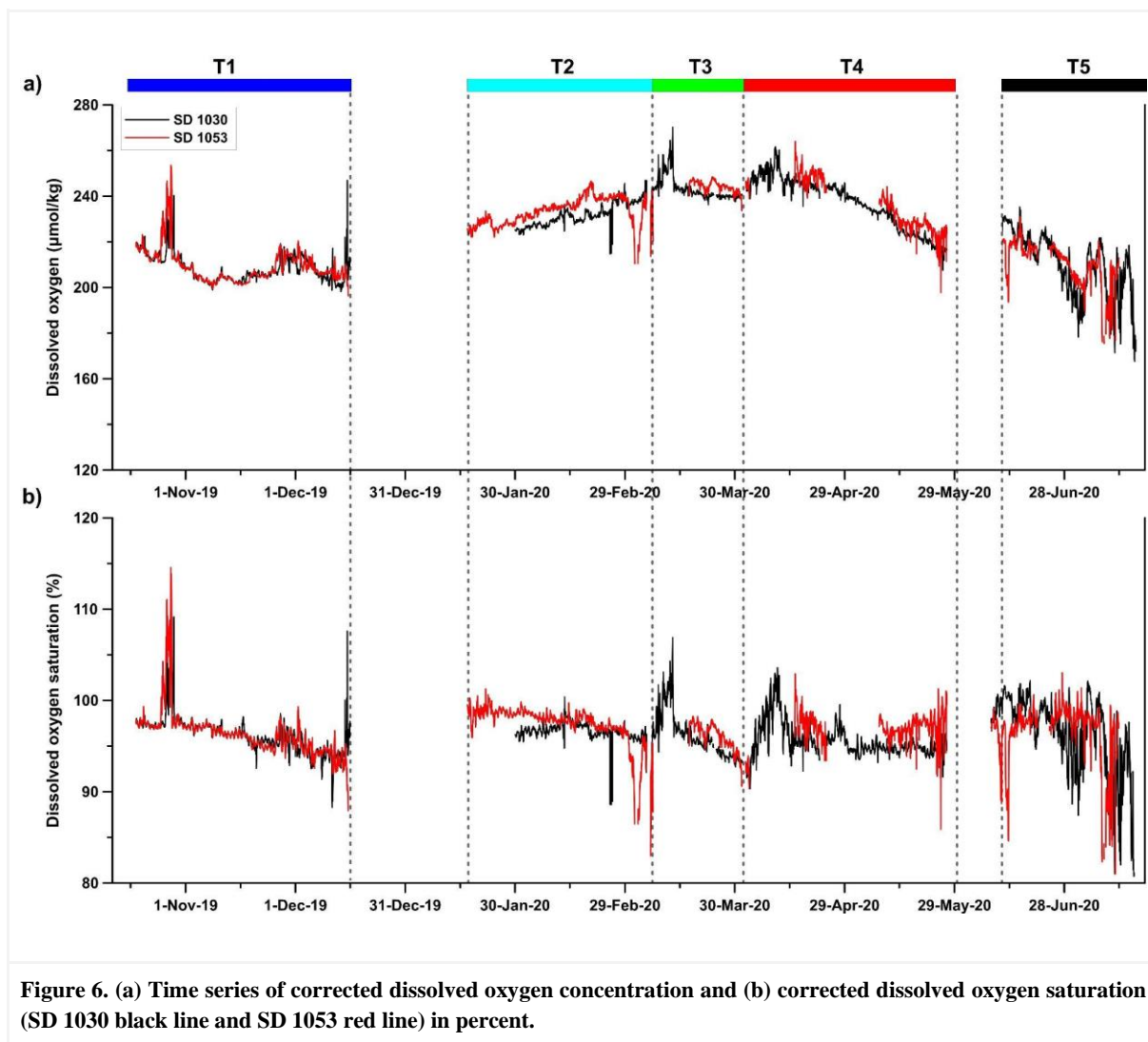
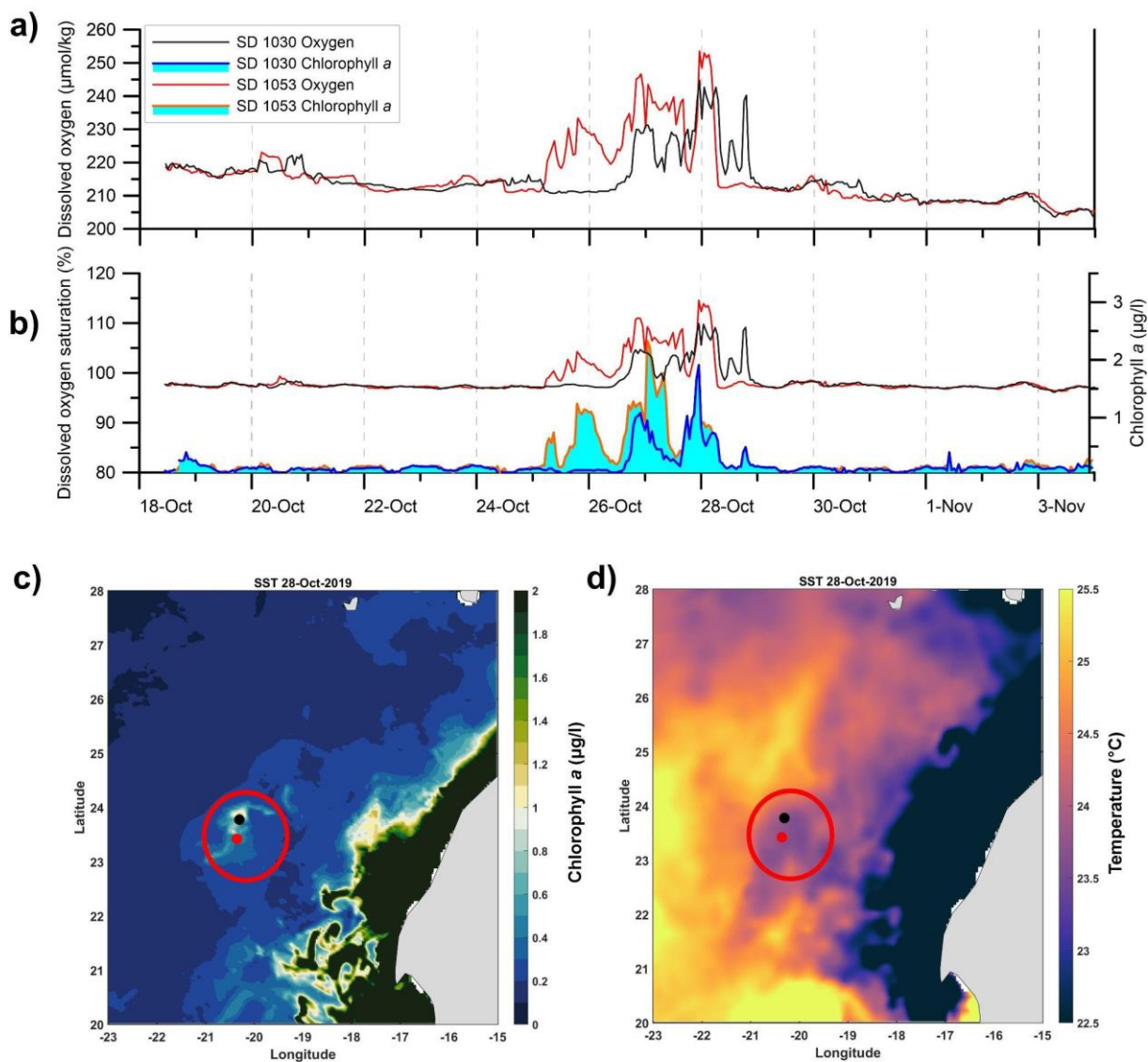


Figure 6. (a) Time series of corrected dissolved oxygen concentration and (b) corrected dissolved oxygen saturation (SD 1030 black line and SD 1053 red line) in percent.

363
364
365
366
367
368
369
370
371

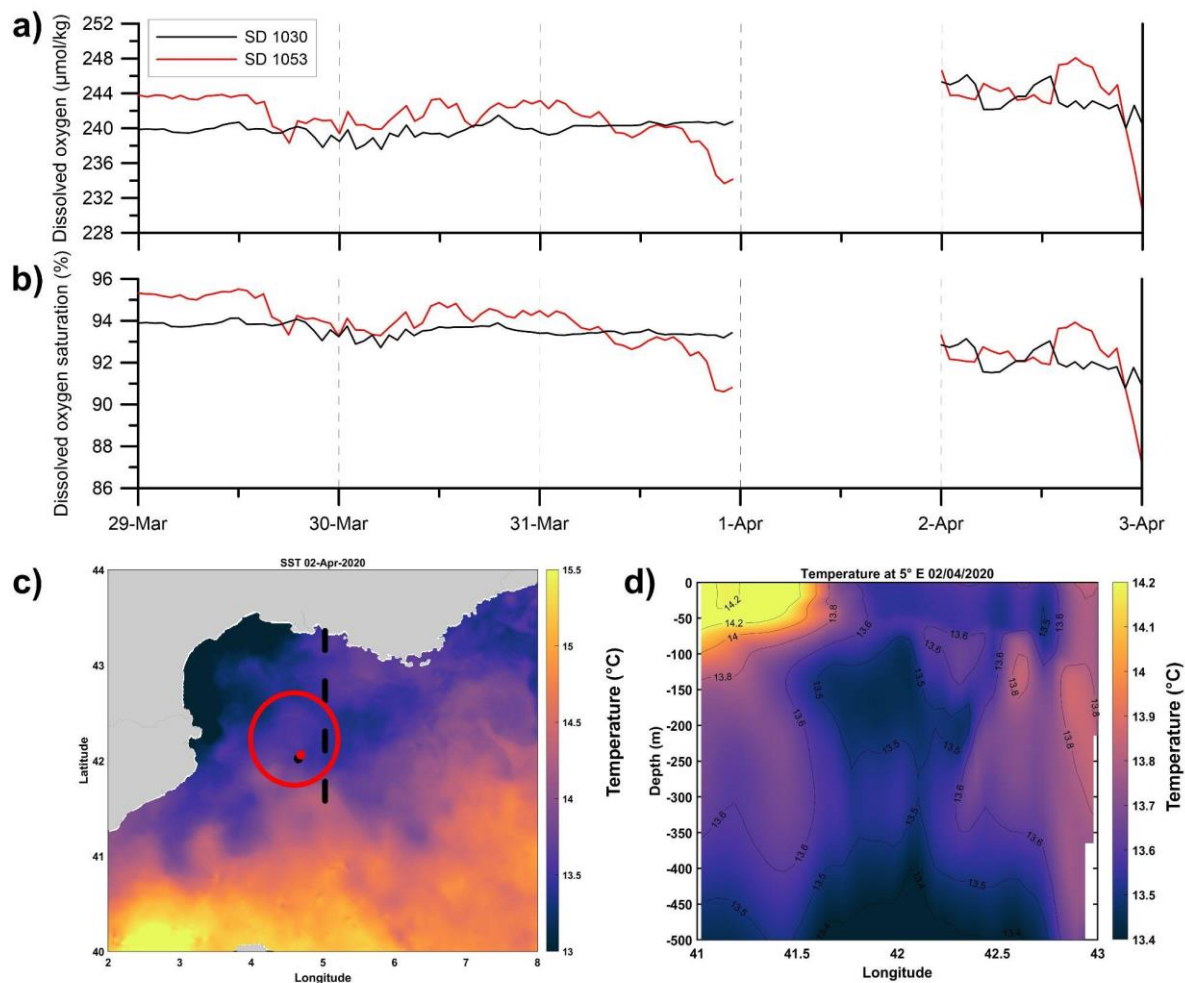
Between October 25 and 29, the dissolved oxygen concentration and saturation were high around the Canary Islands ($>240 \mu\text{mol/kg}$ and $>110\%$; Fig. 7a and b). During the same period high concentrations of Chl-a were measured by SDs ($\sim 2 \mu\text{g/l}$, Fig. 7b, blue and orange line). The area with high Chl-a concentrations off the Canary Islands was visible on the satellite images of sea surface Chl-a concentration (Fig. 7c) and at the same time low sea surface temperature was observed (Fig. 7d). High Chl-a concentrations and low temperatures identify a mesoscale structure that has moved away from the African shelf. Considering that the latter is a very productive area due to the permanent upwelling off NW Africa coast (Cropper et al., 2014; Fischer et al., 2016), this justifies the high Chl-a concentration observed by the SDs at that time.



372
 373
 374
 375
 376
 377
 378

Figure 7. Time series of (a) dissolved oxygen concentration and (b) dissolved oxygen saturation in the Canary Islands area. Sea surface Chl-*a* concentration (c), and (d) sea surface temperature on 28 October 2019. The red circle highlights the position of SDs (black dot = SD1030 and red dot=SD1053).

379



380

381

Figure 8. Time series of (a) dissolved oxygen concentration and (b) percent dissolved oxygen saturation in the Balearic basin. (c) Sea surface temperature evolution between 31 March and 2 April 2020. The black dotted line highlights the vertical section in (d). The red circle highlights the position of SDs (black dot = SD1030 and red dot=SD1053).

384

Between 29 March and 3 April 2020, the SDs crossed the Balearic basin reaching the Gulf of Lion on the 1 April, 2020, the SD 1053 measured a decrease in dissolved oxygen concentrations of about $10 \mu\text{mol/kg}$ (Fig. 8a). This behaviour was also observed in the dissolved oxygen saturation (Fig. 8b) which reached values lower than 95%. The northern part of the basin was characterised by lower surface temperatures (Fig. 8c) than the southern part. The vertical temperature section (Fig. 8d) highlighted the presence of upwelling of cold water to the surface justifying the lower surface temperature observed in Fig. 8c. The presence of this upwelled water caused the decrease in dissolved oxygen saturation (Fig. 8b) observed by the SDs, as the upwelled water is commonly characterised by low dissolved oxygen concentrations due to biological respiration (Chan et al., 2019).

393

394 4.3 $p\text{CO}_2$

395 $p\text{CO}_2$ (μatm) from the ASVCO2 instrument attached to the SD 1030 were calculated according to Sutton et al.
 396 (2014) using T and S from the SBE37-SMP-ODO at the SD. Fig. 9a shows the uncorrected and corrected $p\text{CO}_2$
 397 acquired from the SD 1030. In Fig. 9b, the difference between corrected and uncorrected $p\text{CO}_2$ is shown and the
 398 offset increases from approximately $1 \mu\text{atm}$ at the start of the experiment to approximately $12 \mu\text{atm}$ at the end.

399

400

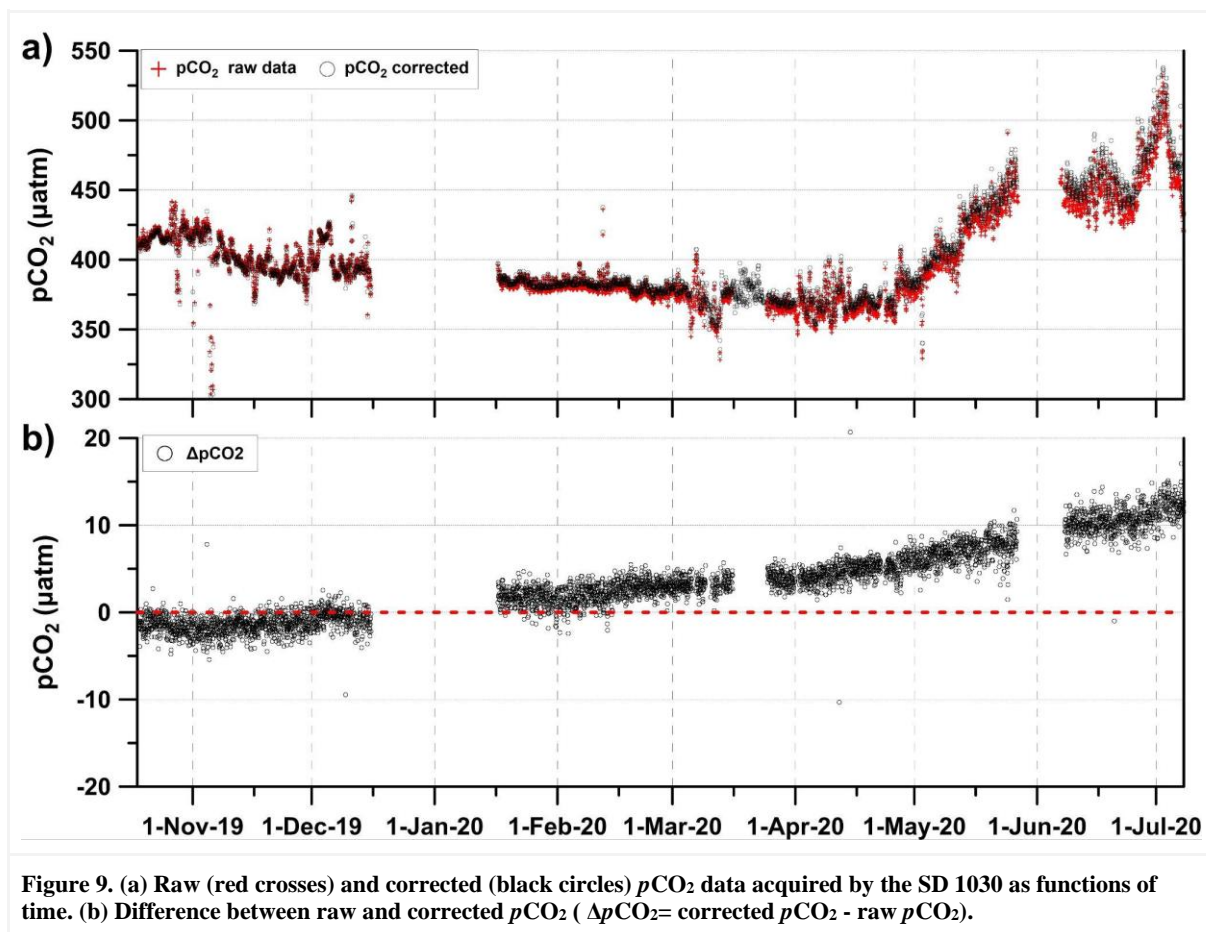


Figure 9. (a) Raw (red crosses) and corrected (black circles) $p\text{CO}_2$ data acquired by the SD 1030 as functions of time. (b) Difference between raw and corrected $p\text{CO}_2$ ($\Delta p\text{CO}_2 = \text{corrected } p\text{CO}_2 - \text{raw } p\text{CO}_2$).

401
 402 The $p\text{CO}_2$ sensors at the different fixed stations were deployed at depths between 2 to 10 m while the SD measured
 403 at 0.5 m depth. To be able to compare $p\text{CO}_2$ measurements from the different depths, the station $p\text{CO}_2$ data were
 404 normalised to surface temperature by using the relationship of Takahashi et al. (1993): $p\text{CO}_2(1) =$
 405 $p\text{CO}_2(2) \exp^{0.0423(T_1 - T_2)}$ (5)
 406 where T is temperature and 1 and 2 refer to the measurements at 0.5 m depth of the SD and at the measurement
 407 depth of each local station, respectively. Furthermore, the $p\text{CO}_2$ measurements acquired by the SD 1030 were
 408 compared to the corrected $p\text{CO}_2$, surface temperature normalised, from the fixed ocean stations (Fig. 10 and Table
 409 2). The difference varied between -0.5 and -16.9 μatm. The largest difference occurred in the eastern Atlantic,
 410 where calculated $p\text{CO}_2$ from discrete DIC and TA were compared to the SD 1030 $p\text{CO}_2$ data. Part of this deviation
 411 is likely attributed to calculation errors which is estimated to be about 10 μatm when errors in both DIC, TA, and
 412 the carbon constants are included (Orr et al., 2018). The smallest difference between the SD 1030 $p\text{CO}_2$ and the
 413 $p\text{CO}_2$ acquired from the fixed stations and normalised to surface temperature are seen at DYFAMED toward the
 414 end of April 2020 (-2.9 μatm) and at MIRAMARE in mid July 2020 (-0.5 μatm). The larger discrepancy at
 415 WIM3A and PALOMA might be attributed to processes which are not taken into account by temperature
 416 normalising, e.g., spatial gradients due to primary production/remineralisation, which would decrease/increase the
 417 $p\text{CO}_2$. However, it is difficult to estimate the impact of these processes.
 418

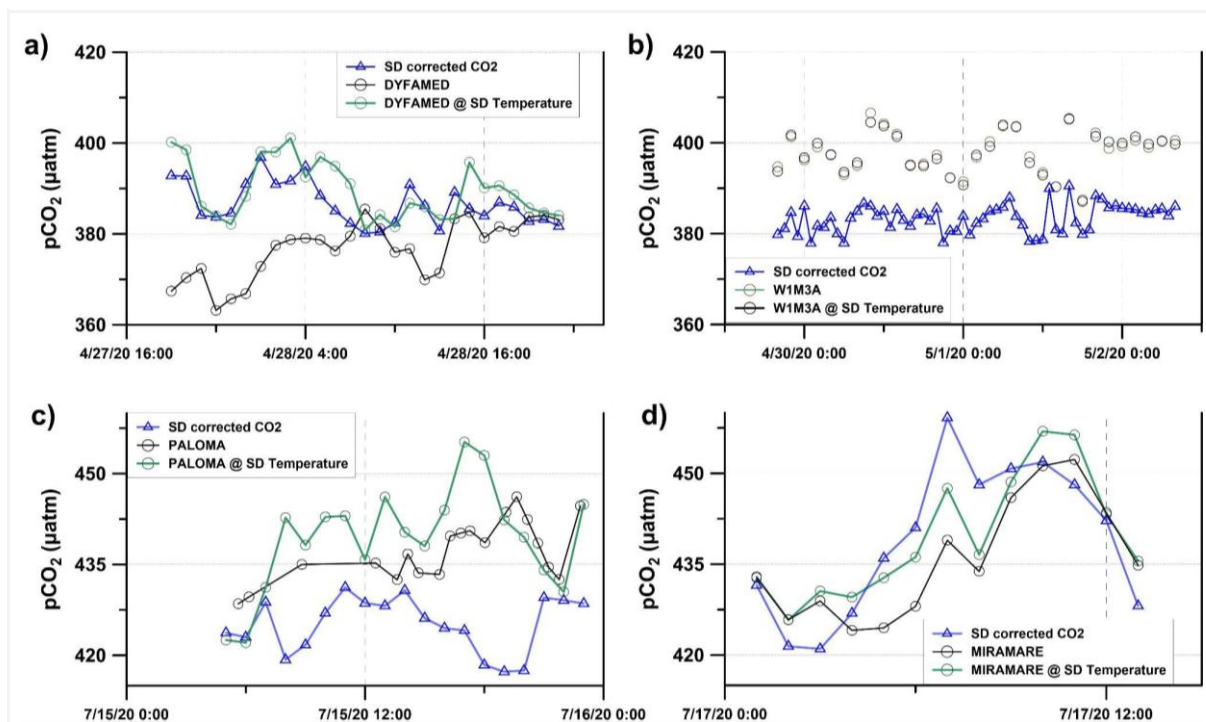


Figure 10. Comparison between $p\text{CO}_2$ measured by the SD 1030 (blue) and at the fixed ocean stations (black and green): the fixed ocean station $p\text{CO}_2$ measured at *in situ* depth and temperature (black) and the fixed ocean station $p\text{CO}_2$ normalised to surface temperature (green). (a) DYFAMED fixed station, (b) W1M3A fixed station, (c) PALOMA fixed station, and (d) MIRAMARE fixed station.

419

420

Table 2. Comparison between $p\text{CO}_2$ measurements at SD 1030 and the fixed ocean stations.

Station/ platform	Measurements	Date	Deviation between $p\text{CO}_2$ at SD 1030 and $p\text{CO}_2$ at fixed station normalised to SST (μatm)
RV Meteor	Discrete DIC and TA samples @ 5 m	30 Nov 2019	-16.9 μatm
DYFAMED	$p\text{CO}_2$ sensor @ 10 m	27-28 Apr 2020	-2.9 μatm
W1M3A	$p\text{CO}_2$ sensor @ 6 m	28 Apr - 2 May 2020	-14.2 μatm
PALOMA	$p\text{CO}_2$ sensor @ 3 m	15 July 2020	-14.7 μatm
MIRAMARE	$p\text{CO}_2$ sensor @ 2 m	17 July 2020	-0.5 μatm

421 SST= sea surface temperature

422

423 5 Summary

424 The ATL2MED demonstration experiment, which lasted for 273 days, represented the first monitoring
 425 experiments of SDs covering both the ETNA region and the Mediterranean Sea, evaluating dynamics between
 426 fixed ocean stations within the same basin as well as comparing characteristics between basins. The experiment
 427 covered all seasons with varying meteorological and oceanographic conditions, primary productivity, and maritime
 428 traffic. The ATL2MED lasted longer than planned primarily due to challenges with heavy biofouling of the two
 429 SDs, COVID-19 pandemic restrictions, low winds, and strong contrary winds.

430 A huge amount of data has been produced during the ATL2MED demonstration experiment, and the data
 431 required quality control and assurance to a varying degree, primarily depending on how sensitive the sensors were
 432 to biofouling. Due to the COVID-19 pandemic restrictions, there was a lack of validation samples collected from

433 cruise transects, Argo floats, and fixed stations, and this has enforced a new way of thinking regarding drift
 434 correction. The SBE salinity data acquired by the SDs have been corrected, when necessary, using model products
 435 and the method was validated by comparing the data corrected with available *in situ* measurements. This resulted
 436 in remarkable consistency of the salinity correction in both space and time. The data from the Aanderaa dissolved
 437 oxygen sensors mounted on the SDs were corrected making use of in air oxygen measurements to correct the trend.
 438 The corrected SD data sets fit well with data from fixed stations and gliders, which means that the correction
 439 methods used are valid. The output is data sets that are available for process interpretations in future research.

440 Other SD sensors were affected by biofouling to such a degree that the data sets were unable to be corrected
 441 given the limited samples available for validation, like *e.g.* the optical sensors for fluorescence measurements.
 442 Some recommendations related to this issue are presented in the next section.

443 The ATL2MED demonstration experiment is an example of how ASV can be used to perform multi-variable
 444 and high-resolution sampling from areas which are not easily accessible, *e.g.* due to remote location, limited
 445 shiptime availability, or COVID-19 restrictions. The SDs are environmentally friendly platforms, and they,
 446 together with other ASV, are useful as a complement in the validation of fixed ocean stations. However, the
 447 experiment clearly shows some of the challenges faced when this type of surface vehicle is part of long-term
 448 missions.
 449

450 **6 Experiences and recommendations**

451 Our experiences and recommendations from the ATL2MED demonstration experiment can be summarised in the
 452 following bullet points, which are explained in more detail at the end of this paragraph:

453 We experienced that

- 454 - the SD sensors were exposed to severe biofouling
- 455 - a substantially amount of effort was required to correct the SD data sets
- 456 - some of the SD sensors were mounted in an unfavourable way
- 457 - the COVID-19 pandemic limited the access to ship time and thus also collection of discrete validation
 458 samples

459 We recommend to:

- 460 - ensure a maintenance and cleaning frequency of the SD sensors and hull which is adapted to the local
 461 environment
- 462 - use biolimiting equipment at the SDs
- 463 - implement an automatic in air calibration procedure for the SD oxygen measurements,
- 464 - ensure that the SD sensors are mounted in such a way that they are exposed to open waters
- 465 - ensure that a sufficient amount of independent measurements (*e.g.*, salinity, dissolved oxygen, carbonate
 466 system, Chl-a) are collected in vicinity of the SD trajectories in order to validate the SD sensors

467 In general, the use of SDs requires a severe amount of effort into securing that the data are of scientifically usable
 468 quality. More specifically, the sensors installed on the SDs always remain in the surface layer and are exposed for
 469 biofouling, which can be particularly impacting in relatively warm waters of the Mediterranean Sea, and not only
 470 during summer. For future experiment, a maintenance and sensor cleaning frequency depending on the area should
 471 be implemented. In situations where this is not possible, biolimiting equipment should be used, like UV systems
 472 powered by the solar panels and wipers which regularly clean the optical sensors. Furthermore, regular cleaning
 473 of the hull will also ensure the necessary manoeuvrability and navigation precision. Experiences from the
 474 ATL2MED demonstration experiment showed that the RBR (<https://rbr-global.com/>) sensor package used on the
 475 SDs had serious issues regarding the biofouling effect. After 9 months in sea, this is somewhat expected. However,
 476 the SBE37 sensors seem to be more reliable and robust regarding biofouling, but a regular sensor cleaning
 477 procedure is necessary using special devices or human interventions during the SD deployment. Regarding
 478 correction of dissolved oxygen, it is advised to facilitate an in air calibration like the one used for Argo floats. This
 479 would require some reorganisation of the sensors, however, it will be easier to correct for drift of the oxygen
 480 sensor. It is also advised to look into the location of the SD sensors. For instance, the RBR sensor on the SD 1053
 481 measured significantly lower dissolved oxygen concentration compared to the SBE. One possible explanation for

482 this could be that the RBR sensor was mounted inside the ship keel where dead water could accelerate the sensor
483 fouling. It must be ensured that the SD sensors are mounted correctly to sample open water.

484 The ATL2MED demonstration experiment suffered from a lack of discrete samples for validation. Thus,
485 future experiments should be organised in such a way that discrete samples for salinity, dissolved oxygen, carbon,
486 and Chl-a are collected at a reasonable frequency, which will ease the validation of the SD data set quality
487 tremendously. Finally, the suitability of SDs as tool to validate other types of measuring devices (*e.g.*, fixed ocean
488 stations, mobile platforms or ships) strongly depends on various conditions such as distance from the platforms,
489 depth of fixed station measurements, environmental conditions and status of the sensors. All these factors need to
490 be carefully considered to ensure the best possible data set for such a validation.

491

492 **Data availability.** Data described in this work is available from different sources, see Table S6 in the
493 Supplementary Material.

494

495 **Supplement.** The supplementary material is available at the end of this manuscript.

496

497 **Author contribution.** RM, ...

498 **Competing interests.** The contact author declares that none of the authors has any competing interests.

499

500 **Acknowledgement**

501 The ATL2MED experiment has received generous funding from the US company PEAK 6 Invest and invaluable
502 support regarding coordination, operation, and data deliverance from Saildrone Inc.. Furthermore, funding has
503 been provided by GEOMAR Helmholtz Centre for Ocean Research (GEOMAR), Integrated Carbon Observation
504 System - Ocean Thematic Centre (ICOS-OTC), the French National Centre for Scientific Research (CNRS),
505 Oceanography Laboratory of Villefranche (LOV), the Oceanic Platform of the Canary Islands (PLOCAN), Ocean
506 Science Centre Mindelo (OSCM), the Hydrographic Institute of Portugal (IH), Balearic Islands Coastal Observing
507 and Forecasting System (SOCIB), Italian National Institute of Oceanography and Applied Geophysics (OGS),
508 Helmholtz Zentrum Geesthacht (HZG), Centre Scientifique de Monaco (CSM), National Research Council-
509 Institute of Marine Sciences (CNR-ISMAR), and National Research Council - Institute for the study of Anthropic
510 Impact and Sustainability in the Marine Environment (CNR-IAS). We thank the OGS engineers Paolo Mansutti
511 and Giuseppe Siena for the assistance during the final recovery of the SDs, and Piero Zuppelli, Riccardo Gerin,
512 Antonio Bussani and Massimo Pacciaroni for piloting the OGS glider. Furthermore, we thank Björn Fiedeler and
513 Benjamin Pfeil for initialising the demonstration experiment and for executing the first phase of the experiment.
514 Finally, we thank Adrienne Sutton and Stacy Manner for invaluable help with correcting the ASVCO₂ *p*CO₂ data.
515

516 **References**

- 517 Bittig, H. C., Körtzinger, A., Neill, C., van Ooijen, E., Plant, J. N., Hahn, J., Johnson, K. S., Jang, B., and Emerson,
518 S. R.: Oxygen optode sensors: principle, characterization, calibration, and application in the ocean, *Front. Mar.*
519 *Sci.*, 4, 429, <https://doi.org/10.3389/fmars.2017.00429>, 2018.
- 520 Bosse, A., Testor, P., Mortier, L., Prieur, L., Taillandier, V., D'Ortenzio, F., and Coppola, L.: Spreading of
521 Levantine Intermediate Waters by submesoscale coherent vortices in the northwestern Mediterranean Sea as
522 observed with gliders, *J. Geophys. Res-Oceans*, 120(3), 1599-1622, <https://doi.org/10.1002/2014JC010263>,
523 2015.

- 524 Bozzano, R., Pensieri, S., Pensieri, L., Cardin, V., Brunetti, F., Bensi, M., Petihakis, G., Tsagaraki, T. M., Ntoumas,
525 M., Podaras, D., and Perivoliotis, L.: The M3A network of open ocean observatories in the Mediterranean Sea,
526 in: 2013 MTS/IEEE OCEANS-Bergen, IEEE, Bergen, Norway, 10-14 June 2013, 1-10, 2013.
- 527 Bozzano, R. and Pensieri, S.: W1M3A fixed station data collected as part of the ATL2MED demonstration
528 experiment 2019-2020 [Data set], <https://hdl.handle.net/11676/Z9bGSnVObyglR0o8zcvmlXBz>, 2024.
- 529 Buongiorno Nardelli, B., Tronconi, C., Pisano, A., and Santoleri, R.: High and Ultra-High resolution processing
530 of satellite Sea Surface Temperature data over Southern European Seas in the framework of MyOcean project,
531 Copernicus Monitoring Environment Marine Service (CMEMS) [Data set], <https://doi.org/10.48670/moi-00172>, 2022.
- 533 Canepa, E., Pensieri, S., Bozzano, R., Faimali, M., Traverso, P., and Cavaleri, L.: The ODAS Italia 1 buoy: More
534 than forty years of activity in the Ligurian Sea, *Progr. Oceanogr.*, 135, 48-63,
535 <https://doi.org/10.1016/j.pocean.2015.04.005>, 2015.
- 536 Cantoni, C., Luchetta, A., Celio, M., Cozzi, S., Raicich, F., and Catalano, G.: Carbonate system variability in the
537 gulf of Trieste (north Adriatic Sea), *Estuar. Coast. Shelf. S.*, 115, 51-62,
538 <https://doi.org/10.1016/j.ecss.2012.07.006>, 2012.
- 539 Cantoni, C. and Luchetta, A.: PALOMA fixed station data collected as part of the ATL2MED demonstration
540 experiment 2019-2020 [Data set], <https://hdl.handle.net/11676/an-PJSKTiEVHj3H0gA8ak3IG>, 2024.
- 541 Capó, E., McWilliams, J. C., Mason, E., and Orfila, A.: Intermittent frontogenesis in the Alboran Sea. *Journal of*
542 *Physical Oceanography*, 51(5), 1417-1439, 2021.
- 543 Cardin, V., Ursella, L., Siena, G., Brunetti, F., Kuchler, S., and Partescano, P.: E2M3A-2017-2019-CTD-time-
544 series-South Adriatic [Data set],
545 <https://nodc.ogs.it/catalogs/doidetails;jsessionid=9D31FDE64403D9BF54F05A1F03D45FB1?0&doi=10.6092/d0d50095-bd30-4ff7-8d0a-a12121e72f78>, 2020.
- 547 Chan, F., Barth, J. A., Kroeker, K. J., Lubchenco, J., and Menge, B. A.: The dynamics and impact of ocean
548 acidification and hypoxia. *Oceanography*, 32(3), 62-71, 2019.
- 549 Civitarese G., Gačić M., Batistić M., Bensi M., Cardin V., Dulčić J., Garić R., Menna M.: The BIOS mechanism:
550 history, theory, implications. *Progress in Oceanography*, 103056. 2023.
- 551 Clayton, T. D. and Byrne, R. H.: Spectrophotometric seawater pH measurements: total hydrogen ion concentration
552 scale calibration of *m*-creosol purple and at-sea results. *Deep-Sea Res.*, 40, 2115-2129, 1993.
- 553 Clementi, E., Aydogdu, A., Goglio, A. C., Pistoia, J., Escudier, R., Drudi, M., Grandi, A., Mariani, A., Lyubartsev,
554 V., Lecci, R., Cretí, S., Coppini, G., Masina, S., and Pinardi, N.: Mediterranean Sea Physical Analysis and
555 Forecast (CMEMS MED-Currents, EAS6 system) (Version 1), Copernicus Monitoring Environment Marine
556 Service (CMEMS) [Data set],
557 https://doi.org/10.25423/CMCC/MEDSEA_ANALYSISFORECAST_PHY_006_013_EAS7, 2021.
- 558 Coppola, L., Raimbault, P., Mortier, L., and Testor, P.: Monitoring the environment in the northwestern
559 Mediterranean Sea, *Eos*, 100, <https://doi.org/10.1029/2019EO125951>, 2019.
- 560 Coppola, L., Diamond, R. E., Carval, T., Irissou J. O., and Desnos, C.: Dyfamed observatory data, SEANOE [Data
561 set], <https://doi.org/10.17882/43749>, 2023.
- 562 Cropper, T. E., Hanna, E., and Bigg, G. R.: Spatial and temporal seasonal trends in coastal upwelling off Northwest
563 Africa, 1981-2012, *Deep-Sea Res. Pt. I*, 86, 94-111, <https://doi.org/10.1016/j.dsr.2014.01.007>, 2014.
- 564 Delauney, L., Compère, C., and Lehaitre, M.: Biofouling protection for marine environmental sensors, *Ocean Sci.*,
565 6, 503-511, <https://doi.org/10.5194/os-6-503-2010>, 2010.
- 566 Delory, E., and Jay P., (Eds.): Challenges and Innovations in Ocean *In Situ* Sensors: Measuring Inner Ocean
567 Processes and Health in the Digital Age. Elsevier, 408 pp, ISBN: 9780128098868, 2018.
- 568 Dickson, A. G.: Standard potential of the reaction: $\text{AgCl}(s) + \frac{1}{2}\text{H}_2(g) = \text{Ag}(s) + \text{HCl}(aq)$, and the standard acidity
569 constant of the ion HSO_4^- in synthetic sea water from 273.15 to 318.15 K, *J. Chem. Thermodyn.*, 22, 113-
570 127, [https://doi.org/10.1016/0198-0149\(90\)90004-F](https://doi.org/10.1016/0198-0149(90)90004-F), 1990.
- 571 Dickson, A. G. and Goyet, C.: Handbook of methods for the analysis of the various parameters of the carbon
572 dioxide system in sea water. Version 2, Oak Ridge National Lab. (ORNL), <https://doi.org/10.2172/10107773>,
573 1994.
- 574 Dickson, A. G., Sabine, C. L., and Christian, J. R. (Eds): Guide to best practices for ocean CO2 measurements,
575 PICES Special Publication 3, North Pacific Marine Science Organization Sidney, British Columbia, 191,
576 <https://doi.org/10.25607/OBP-1342>, 2007.

- 577 Edmond, J. M. . High precision determination of titration alkalinity and total carbon dioxide content of sea water
578 by potentiometric titration. In *Deep Sea Research and Oceanographic Abstracts* (Vol. 17, No. 4, pp. 737-750).
579 Elsevier. 1970.
- 580 Escudier, R., Clementi, E., Cipollone, A., Pistoia, J., Drudi, M., Grandi, A., Lyubartsev, V., Lecci, R., Aydogdu,
581 A., Delrosso, D., Omar, M., Masina, S., Coppini, G., and Pinardi, N.: A High Resolution Reanalysis for the
582 Mediterranean Sea, *Front. Earth Sci.*, 9, <https://doi.org/10.3389/feart.2021.702285>, 2021.
- 583 Escudier, R., Clementi, E., Omar, M., Cipollone, A., Pistoia, J., Aydogdu, A., Drudi, M., Grandi, A., Lyubartsev,
584 V., Lecci, R., Cretí, S., Masina, S., Coppini, G., and Pinardi, N.: Mediterranean Sea Physical Reanalysis
585 (CMEMS MED-Currents) (Version 1) [Data set], Copernicus Monitoring Environment Marine Service
586 (CMEMS), https://doi.org/10.25423/CMCC/MEDSEA_MULTIYEAR_PHY_006_004_E3R1I, 2020.
- 587 Fischer, G., Romero, O., Merkel, U., Donner, B., Iversen, M., Nowald, N., Ratmeyer, V., Ruhland, G., Klann, M.,
588 and Wefer, G.: Deep ocean mass fluxes in the coastal upwelling off Mauritania from 1988 to 2012: variability
589 on seasonal to decadal timescales, *Biogeosciences*, 13, 3071–3090, <https://doi.org/10.5194/bg-13-3071-2016>,
590 2016.
- 591 Friederich, G. E., Brewer, P. G., Herlien, R., and Chavez, F. P.: Measurement of sea surface partial pressure of
592 CO₂ from a moored buoy, *Deep-Sea Res. Pt. I*, 42, 1175–1186, [https://doi.org/10.1016/0967-0637\(95\)00044-](https://doi.org/10.1016/0967-0637(95)00044-7)
593 7, 1995.
- 594 Gačić, M., Ursella, L., Kovačević, V., Menna, M., Malačič, V., Bensi, M., Negretti, M.-E., Cardin, V., Mirko
595 Orlić, M., Sommeria, J., Barreto, R. V., Viboud, S., Valran, T., Petelin, B., Siena, G., and Rubino, A.: Impact
596 of dense-water flow over a sloping bottom on open-sea circulation: laboratory experiments and an Ionian Sea
597 (Mediterranean) example. *Ocean Sci.*, 17, 975–996, <https://doi.org/10.5194/os-17-975-2021>, 2021.
- 598 Garcia, H. E. and Gordon, L. I.: Oxygen solubility in seawater: Better fitting equations, *Limnol. Oceanogr.*, 37 (6),
599 1307-1312, 1992.
- 600 GDAC: <ftp://ftp.ifremer.fr/argo>, last access 17-10-2023.
- 601 Gentemann, C. L., Scott, J. P., Mazzini, P. L. F., Pianca, C., Akella, S., Minnett, P. J., Cornillon, P., Fox-Kemper,
602 B., Cetinić, I., Chin, T. M., Gomez-Valdes, J., Vazquez-Cuervo, J., Tsonos, V., Yu, L., Jenkins, R., De
603 Halleux, S., Peacock, D., and Cohen, N.: Salidrone - Adaptively sampling the marine environment, BAMS,
604 <https://doi.org/10.1175/BAMS-D-19-0015.1>, 2020.
- 605 Gerin, R., Bussani, A., Kuchler, S., Martellucci, R., Pacciaroni, M., Pirro, A., Zuppelli, P., and Mauri, E: OGS
606 GLIDER MISSION Convex20 Dataset [Data set], 2021.
- 607 Giani, M.: MIRAMARE fixed station data collected as part of the ATL2MED demonstration experiment 2019-
608 2020 [Data set], <https://hdl.handle.net/11676/ngPlu-Q0dtDcDx2wMFTNOtnZ>, 2024.
- 609 Glueckauf, E.: The Composition of Atmospheric Air, In: *Compendium of Meteorology*, edited by: Malone, T.F.,
610 American Meteorological Society, Boston, MA., 3-10, https://doi.org/10.1007/978-1-940033-70-9_1, 1951.
- 611 Gonzalez, A. I. and Bruno, M.: Data from RV Ucadiz, 5-6 March 2020 [Dataset], [https://fileshare.icos-](https://fileshare.icos-cp.eu/s/eyLp9m685QA8ME7)
612 [cp.eu/s/eyLp9m685QA8ME7](https://fileshare.icos-cp.eu/s/eyLp9m685QA8ME7), 2024.
- 613 Gordon, A. L. and Giulivi, C. F.: Ocean eddy freshwater flux convergence into the North Atlantic subtropics.
614 *Journal of Geophysical Research: Oceans*, 119(6), 3327-3335, 2014.
- 615 Hernandez-Ayon, J. M., Belli, S. L., Zirino, A.: pH, alkalinity and total CO₂ in coastal seawater by potentiometric
616 titration with a difference derivative readout, *Anal. Chim. Acta* 394, 101–108, 1999.
- 617 Johnson, K. M., Wills, K. D., Butler, D. B., Johnson, W. K. and Wong, C. S.: Coulometric total carbon dioxide
618 analysis for marine studies, *Mar. Chem.*, 44, 167-187, 1993.
- 619 Johnson, K. S., Plant, J. N., Riser, S. C., and Gilbert, D.: Air oxygen calibration of oxygen optodes on a profiling
620 float array, *J. Atmos. Ocean. Tech.*, 32, 2160-2172, <https://doi.org/10.1175/JTECH-D-15-0101.1>, 2015.
- 621 Kokkini, Z., Mauri, E., Gerin, R., Poulain, P.-M., Simoncelli, S., and Notarstefano, G.: On the salinity structure in
622 the South Adriatic as derived from float and glider observations in 2013–2016, *Deep-Sea Res. Pt. II*, 171,
623 104625, <https://doi.org/10.1016/j.dsr2.2019.07.013>, 2019.
- 624 Lee, K., Kim, T.-W., Byrne, R. H., Millero, F. J., Feely, R. A., and Liu, Y.-M.: The universal ratio of boron to
625 chlorinity for the North Pacific and North Atlantic oceans, *Geochim. Cosmochim. Acta*, 74, 1801–1811,
626 <https://doi.org/10.1016/j.gca.2009.12.027>, 2010.
- 627 Lueker, T. J., Dickson, A. G., and Keeling, C. D.: Ocean pCO₂ calculated from dissolved inorganic carbon,
628 alkalinity, and equations for K₁ and K₂: validation based on laboratory measurements of CO₂ in gas and
629 seawater at equilibrium, *Mar. Chem.*, 70, 105-119, [https://doi.org/10.1016/S0304-4203\(00\)00022-0](https://doi.org/10.1016/S0304-4203(00)00022-0), 2000.

- 630 Martellucci, R., Salon, S., Cossarini, G., Piermattei, V., and Marcelli, M.: Coastal phytoplankton bloom
 631 dynamics in the Tyrrhenian Sea: Advantage of integrating *in situ* observations, large-scale analysis and forecast
 632 systems, *J. Marine Syst.*, 218, 103528, <https://doi.org/10.1016/j.jmarsys.2021.103528>, 2021.
- 633 Mauri, E., Gerin, R., and Poulain, P.-M.: Measurements of water-mass properties with a glider in the South-
 634 western Adriatic Sea, *J. Oper. Oceanogr.*, 9, sup1, s3-s9, <https://doi.org/10.1080/1755876X.2015.1117766>,
 635 2016.
- 636 Menna, M., Gačić, M., Martellucci, R., Notarstefano, G., Fedele, G., Mauri, E., Gerin, R., and Poulain, P. M.
 637 Climatic, decadal, and interannual variability in the upper layer of the Mediterranean Sea using remotely sensed
 638 and in-situ data. *Remote Sensing*, 14(6), 1322, 2022.
- 639 Menna, M., Martellucci, R., Reale, M., Cossarini, G., Salon, S., Notarstefano, G., Mauri, E., Poulain, P.-M., Gallo,
 640 A., and Solidoro, C.: Impacts of an extreme weather system on the oceanographic features of the Mediterranean
 641 Sea: the Medicane Apollo, *Sci. Rep-UK*, 13, 3870, <https://doi.org/10.1038/s41598-023-29942-w>, 2023.
- 642 Merchant, C. J., Embury, O., Bulgin, C. E., Block, T., Corlett, G. K., Fiedler, E., Good, S.A., Mittaz, J., Rayner,
 643 N.A., Berry, D., Eastwood, S., Taylor, M., Tsushima, Y., Waterfall, A., Wilson R., Donlon, C.. Satellite-based
 644 time-series of sea-surface temperature since 1981 for climate applications. *Scientific data*, 6(1), 223. 2019.
- 645 Merlivat, L., and Brault, P.: CARIOCA Buoy: Carbon Dioxide Monitor, *Sea Technol.*, 23–30, 1995.
- 646 Merlivat, L., Boutin, J., Antoine, D., Beaumont, L., Golbol, M., and Vellucci, V.: Increase of dissolved inorganic
 647 carbon and decrease in pH in near-surface waters in the Mediterranean Sea during the past two decades,
 648 *Biogeosciences*, 15, 5653–5662, <https://doi.org/10.5194/bg-15-5653-2018>, 2018.
- 649 Mihanović, H., Vilibić, I., Šepić, J., Matić, F., Ljubešić, Z., Mauri, E., Gerin, R., Notarstefano, G., and Poulain,
 650 P.-M.: Observation, Preconditioning and Recurrence of Exceptionally High Salinities in the Adriatic Sea,
 651 *Front. Mar. Sci.* 8, 834. <https://doi.org/10.3389/fmars.2021.672210>, 2021.
- 652 Neri, F., Romagnoli, T., Accoroni, S., Ubaldi, M., Garzia, A., Pizzuti, A., Campanelli, A., Grilli, F., Marini, M.,
 653 and Totti, C.: Phytoplankton communities in a coastal and offshore stations of the northern Adriatic Sea
 654 approached by network analysis and different statistical descriptors, *Estuarine, Coastal and Shelf Science*, 282,
 655 108224, 2023.
- 656 Orr, J. C., Epitalon, J.-M., Dickson, A. G., and Gattuso, J.-P.: Routine uncertainty propagation for the marine
 657 carbon dioxide system, *Mar. Chem.*, 207, 84-107, <https://doi.org/10.1016/j.marchem.2018.10.006>, 2018.
- 658 Pastor, F., Valiente, J. A., and Palau, J. L.: Sea surface temperature in the Mediterranean: Trends and spatial
 659 patterns (1982–2016). *Meteorology and climatology of the Mediterranean and Black Seas*, 297-309, 2019.
- 660 Paulsen, M. et al.: Data from RV Meteor 30 November, 2019 [Dataset], [https://fileshare.icos-](https://fileshare.icos-cp.eu/s/eyLp9m685QA8ME7)
 661 [cp.eu/s/eyLp9m685QA8ME7](https://fileshare.icos-cp.eu/s/eyLp9m685QA8ME7), 2023.
- 662 Pelletier, G., Lewis, E., and Wallace, D.: CO2SYS.XLS: A calculator for the CO2 system in seawater for Microsoft
 663 Excel/VBA, Wash. State Dept. of Ecology/Brookhaven Nat. Lab., Olympia, WA/Upton, NY, USA, 2007.
- 664 Perez, F. F. and Fraga, F.: Association constant of fluoride and hydrogen ions in seawater, *Mar. Chem.*, 21, 161–
 665 168, [https://doi.org/10.1016/0304-4203\(87\)90036-3](https://doi.org/10.1016/0304-4203(87)90036-3), 1987.
- 666 Pinardi, N.; Cessi, P.; Borile, F.; Wolfe, C. The Mediterranean Sea Overturning Circulation. *J. Phys. Oceanogr.*
 667 2019, 49, 1699–1721. 2019.
- 668 Pirro, A., Mauri, E., Gerin, R., Martellucci, R., Zuppelli, P., and Poulain, P.-M.: New insights on the formation
 669 and breaking mechanism of convective cyclonic cones in the South Adriatic Pit during winter 2018, *J. Phys.*
 670 *Oceanogr.*, 52, 2049–2068, <https://doi.org/10.1175/JPO-D-21-0108.1>, 2022.
- 671 Poulain, P.-M., Centurioni, L., Özgökmen, T., Tarry, D., Pascual, A., Ruiz, S., Mauri, E., Menna, M., Notarstefano,
 672 G.: On the Structure and Kinematics of an Algerian Eddy in the Southwestern Mediterranean Sea. *Remote*
 673 *Sensing*, 13(15):3039. <https://doi.org/10.3390/rs13153039>, 2021.
- 674 Pranić, P., Denamic, C., Janeković, I., and Vilibić, I.: Multi-model analysis of the Adriatic dense-water dynamics,
 675 *Ocean Science*, 19(3), 649-670, 2023.
- 676 Ravaioli, M., Bergami, C., Riminucci, F., Langone, L., Cardin, V., Di Sarra, A., Aracri, S., Bastianini, M., Bensi,
 677 M., Bergamasco, A., Bommarito, C., Borghini, M., Bortoluzzi, G., Bozzano, R., Cantoni, C., Chiggiato, J.,
 678 Crisafi, E., D'Adamo, R., Durante, S., Fanara, C., Grilli, F., Lipizer, M., Marini, M., Miseroocchi, S., Paschini,
 679 E., Penna, P., Pensieri, S., Pugnetti, A., Raicich, F., Schroeder, K., Siena, G., Specchiulli, A., Stanghellini, G.,
 680 Vetrano, A., and Crise, A.: The RITMARE Italian Fixed-Point Observatory Network (IFON) for marine
 681 environmental monitoring: a case study, *J. Oper. Oceanogr.*, 9: sup1, s202-s214,
 682 <https://doi.org/10.1080/1755876X.2015.1114806>, 2016.

- 683 Reverdin, G., Kestenare, E., Frankignoul, C., and Delcroix, T.: Surface salinity in the Atlantic Ocean (30 S–50 N).
 684 *Progress in Oceanography*, 73(3-4), 311-340, 2007.
- 685 Skjelvan, I., Coppola, L., Cardin, V., Juza, M., Bozzano, R., Pensieri, S., Giani, M., Siena, G., Urbini, L., Mauri,
 686 E., Martellucci, R., Cantoni, C., Luchetta, A., Izquierdo, A., Paulsen, M., and Fiedler, B.: The ATL2MED
 687 mission - experiences and lessons learnt, Technical report, ICOS-OTC, <https://doi.org/10.18160/9HK5-807K>,
 688 2021.
- 689 Skjelvan, I. and Fiedler, B.: Data from Saildrone 1030 during the ATL2MED demonstration experiment 2019-
 690 2020 [Data set], <https://hdl.handle.net/11676/mxGAeRL4UPrNdz08p7dBxVpR>, 2024.
- 691 Skjelvan, I. and Fiedler, B.: Data from Saildrone 1053 during the ATL2MED demonstration experiment 2019-
 692 2020 [Data set], https://hdl.handle.net/11676/4pHG8h6rGfWn_KvLSqgR1iau, 2024.
- 693 Steinhoff, T., Gkritzalis, T., Lauvset S. K., Jones, S., Schuster, U., Olsen, A., Becker, M., Bozzano, R., Brunetti, F.,
 694 Cantoni, C., Cardin, V., Diverrès, D., Fiedler, B., Fransson, A., Giani, M., Hartman, S., Hoppema, M.,
 695 Jeansson, E., Johannessen, T., Kitidis, V., Körtzinger, A., Landa, C., Lefèvre, N., Luchetta, A., Naudts, L.,
 696 Nightingale, P. D., Omar, A. M., Pensieri, S., Pfeil, B., Castaño-Primo, R., Rehder, G., Rutgersson, A., Sanders,
 697 R., Schewe, I., Siena, G., Skjelvan, I., Soltwedel, T., van Heuven, S., and Watson, A.: Constraining the Oceanic
 698 Uptake and Fluxes of Greenhouse Gases by Building an Ocean Network of Certified Stations: The Ocean
 699 Component of the Integrated Carbon Observation System, *ICOS-Oceans, Frontiers in Marine Science*, vol. 6,
 700 p. 544, doi:10.3389/fmars.2019.00544, 2019.
- 701 Sutton, A. J., Sabine, C. L., Maenner-Jones, S., Lawrence-Slavas, N., Meinig, C., Feely, R. A., Mathis, J. T.,
 702 Musielewicz, S., Bott, R., McLain, P. D., Fought, J., and Kozyr, A.: A high-frequency atmospheric and
 703 seawater pCO₂ data set from 14 open ocean sites using a moored autonomous system, *Earth Sys. Sci. Data*, 6,
 704 353–366, <https://doi.org/10.5194/essd-6-353-2014>, 2014.
- 705 Takahashi, T., Olafsson, J., Goddard, J. G., Chipman, D. W., and Sutherland, S. C.: Seasonal variation of CO₂ and
 706 nutrients in the high-latitude surface oceans: a comparative study, *Glob. Biogeochem. Cy.*, 7, 843-878,
 707 <https://doi.org/10.1029/93GB02263>, 1993.
- 708 Takeshita, Y., Martz, T. R., Johnson, K. S., Plant, J. N., Gilbert, D., Riser, S. C., Craig, N. Tilbrook, B. (2013). A
 709 climatology-based quality control procedure for profiling float oxygen data. *Journal of Geophysical Research:*
 710 *Oceans*, 118(10), 5640-5650.
- 711 Tanhua, T., McCurdy, A., Fischer, A., Appeltans, W., Bax, N., Currie, K., DeYoung, B., Dunn, D., Heslop, E.,
 712 Glover, L.K., Gunn, J., Hill, K., Ishii, M., Legler, D., Lindstrom, E., Miloslavich, P., Moltmann, T., Nolan, G.,
 713 Palacz, A., Simmons, S., Sloyan, B., Smith, L.M., Smith, N., Telszewski, M., Visbeck, M., and Wilkin, J.:
 714 What We Have Learned From the Framework for Ocean Observing: Evolution of the Global Ocean Observing
 715 System. *Front. Mar. Sci.* 6:471. doi: 10.3389/fmars.2019.0047, 2019.
- 716 Testor, P., Mortier, L., Coppola, L., Claustre, H., D'Ortenzio, F., Bourrin, F., Durrieu de Madron, X., and
 717 Raimbault, P., Glider MOOSE sections [data set], <https://www.seanoe.org/data/00409/52027/>, 2017.
- 718 Testor, P., de Young, B., Rudnick, D. L., Glenn, S., Hayes, D., Lee, C. M., Pattiaratchi, C., Hill, K., Heslop, E.,
 719 Turpin, V., Alenius, P., Barrera, C., Barth, J. A., Beaird, N., Bécu, G., Bosse, A., Bourrin, F., Brearley, J. A.,
 720 Chao, Y., Chen, S., Chiggiato, J., Coppola, L., Crout, R., Cummings, J., Curry, B., Curry, R., Davis, R., Desai,
 721 K., DiMarco, S., Edwards, C., Fielding, S., Fer, I., Frajka-Williams, E., Gildor, H., Goni, G., Gutierrez, D.,
 722 Haugan, P., Hebert, D., Heiderich, J., Henson, S., Heywood, K., Hogan, P., Houpert, L., Huh, S., Inall, E.,
 723 Ishii, M., Ito, S.-i., Itoh, S., Jan, S., Kaiser, J., Karstensen, J., Kirkpatrick, B., Klymak, J., Kohut, J., Krahnemann,
 724 G., Krug, M., McClatchie, S., Marin, F., Mauri, E., Mehra, A., Meredith, P., Meunier, T., Miles, T., Morell, J.
 725 M., Mortier, L., Nicholson, S., O'Callaghan, J., O'Conchubhair, D., Oke, P., Pallàs-Sanz, E., Palmer, M., Park,
 726 J., Perivoliotis, L., Poulain, P.-M., Perry, R., Queste, B., Rainville, L., Rehm, E., Roughan, M., Rome, N.,
 727 Ross, T., Ruiz, S., Saba, G., Schaeffer, A., Schönau, M., Schroeder, K., Shimizu, Y., Sloyan, B. M., Smeed,
 728 D., Snowden, D., Song, Y., Swart, S., Tenreiro, M., Thompson, A., Tintore, J., Todd, R. E., Toro, C., Venables,
 729 H., Wagawa, T., Waterman, S., Watlington, R. A., and Wilson, D.: OceanGliders: A component of the
 730 integrated GOOS, *Front. Mar. Sci.*, 6, <https://doi.org/10.3389/fmars.2019.00422>, 2019.
- 731 Ulses, C., Estournel, C., Fourrier, M., Coppola, L., Kessouri, F., Lefèvre, D., and Marsaleix, P.: Oxygen budget
 732 of the north-western Mediterranean deep- convection region, *Biogeosciences*, 18, 937–960,
 733 <https://doi.org/10.5194/bg-18-937-2021>, 2021.

734 Wong, A. P. S., Wijffels, S. E., Riser, S. C., Pouliquen, S., Hosoda, S., Roemmich, D., Gilson, J., Johnson, G. C.,
 735 Martini, K., Murphy, D. J., Scanderbeg, M., Bhaskar, T. V. S. U., Buck, J. J. H., Merceur, F., Carval, T., Maze,
 736 G., Cabanes, C., André, X., Poffa, N., Yashayaev, I., Barker, P. M., Guinehut, S., Belbéoch, M., Ignaszewski,
 737 M., Baringer, M. O. N., Schmid, C., Lyman, J. M., McTaggart, K. E., Purkey, S. G., Zilberman, N., Alkire, M.
 738 B., Swift, D., Owens, W. B., Jayne, S. R., Hersh, C., Robbins, P., West-Mack, D., Bahr, F., Yoshida, S., Sutton,
 739 P. J. H., Cancouët, R., Coatanoan, C., Dobbler, D., Juan, A. G., Gourrion, J., Kolodziejczyk, N., Bernard, V.,
 740 Bourlès, B., Claustre, H., D'Ortenzio, F., Le Reste, S., Le Traon, P. Y., Rannou, J. P., Saout-Grit, C., Speich,
 741 S., Thierry, V., Verbrugge, N., Angel-Benavides, I. M., Klein, B., Notarstefano, G., Poulain, P. M., Vélez-
 742 Belchí, P., Suga, T., Ando, K., Iwasaka, N., Kobayashi, T., Masuda, S., Oka, E., Sato, K., Nakamura, T., Sato,
 743 K., Takatsuki, Y., Yoshida, T., Cowley, R., Lovell, J. L., Oke, P. R., van Wijk, E. M., Carse, F., Donnelly, M.,
 744 Gould, W. J., Gowers, K., King, B. A., Loch, S. G., Mowat, M., Turton, J., Rama Rao, E. P., Ravichandran,
 745 M., Freeland, H. J., Gaboury, I., Gilbert, D., Greenan, B. J. W., Ouellet, M., Ross, T., Tran, A., Dong, M., Liu,
 746 Z., Xu, J., Kang, K. R., Jo, H. J., Kim, S. D., and Park, H. M.: Argo Data 1999–2019: Two Million
 747 Temperature-Salinity Profiles and Subsurface Velocity Observations From a Global Array of Profiling Floats,
 748 Front. Mar. Sci., 7, 700, <https://doi.org/10.3389/fmars.2020.00700>, 2020.
 749
 750
 751

752 Supplementary material

754 Table S1. Harbours and dates of SD maintenance, of which all took place in 2020.

Drone	Place	Mindelo (CV)	Telde, Gran Canaria (ES)	Porquerolles (FR)	Imperia (IT)	Cefalù, Sicily (IT)
SD 1030			12 February	22-23 April		26 May - 6 June
SD 1053		4-14 January			7 May	26 May - 6 June

755
 756 Table S2. Instruments, sensors, accuracy, and associated measurement frequency at the different fixed ocean stations,
 757 gliders, and ship during the ATL2MED demonstration experiment.

Instrument/ sensor	Company/ reference	Variable	Accuracy	Measurement frequency	Used by
SBE37	Sea-Bird Scientific	T Cond	0.002°C, 0.0003 S/m	10/min	DYFAMED
SBE41 (GPCTD)	Sea-Bird Scientific	T Cond	0.002°C, 0.0003 S/m	1/s	Glider MOOSE T00
SBE19	Sea-Bird Scientific.	T Cond	0.005°C, 0.0005 S/m	2/day	MIRAMARE
SBE16 plus v2	Sea-Bird Scientific	T Cond	0.005°C, 0.0005 S/m	12/day	W1M3A
SBE41 (GPCTD)	Sea-Bird Scientific	T Cond	0.002°C, 0.0003 S/m	1/s	Glider South Adriatic
SBE37-SMP-ODO	Sea-Bird Scientific	T Cond O ₂	0.002°C, 0.0003 S/m, 3 µmol/kg	15/min 60/min	PALOMA, MIRAMARE
CARIOCA	Merlivat and Brault (1995)	pCO ₂	2 µatm	24/day	DYFAMED

CO ₂ -proCV	Pro-Oceanus Systems Inc	<i>p</i> CO ₂	2 µatm	12/day 6/day 24/day	W1M3A E2M3A MIRAMARE
Contros HydroC	4H-JENA engineering GmbH	<i>p</i> CO ₂	2 µatm	1/min	PALOMA
SBE21	Sea-Bird Scientific	Cond	0.001 S/m	2/min	RV Ucadiz

758 T= temperature; Cond=conductivity; O₂=dissolved oxygen; *p*CO₂=partial pressure of carbon dioxide.

759

760 **Table S3. Instruments and sensors at the SDs from Saldrone Inc. during the ATL2MED demonstration experiment**
761 **and used in this work.**

Instrument/ sensor	Company/ reference	Variable	Accuracy	Measurement frequency
SBE37-SMP-ODO (SD 1030; SD 1053)	Sea-Bird Scientific	T Cond O ₂	0.002°C, 0.0003 S/m, 3 µmol/kg	10/min
ASVCO2 (SD 1030)	PMEL, Sutton et al. (2014)	<i>p</i> CO ₂	2 µatm	24/day

762 T= temperature; Cond=conductivity; O₂=dissolved oxygen; *p*CO₂=partial pressure of carbon dioxide.

763

764 **Table S4. Instruments and methods used to analyse discrete samples collected at the RV Meteor and from different**
765 **fixed stations during the ATL2MED demonstration experiment.**

Instrument/ sensor	Company/ reference (SOP)	Variable	Accuracy	# measurements (depth)	Facility
Simultaneous potentiometric acid titration using a closed cell	SNAPO-CO ₂ prototype, Edmond (1970), Dickson and Goyet (1994)	DIC, TA	± 2 to 5 µmol/kg	1 (5 m)	DYFAMED
SOMMA	UiC (SOP 2), Johnson (1993)	DIC	2 µmol/kg	1 (5 m)	GEOMAR
VINDTA 3S/VINDTA 3C	MARIANDA (SOP 3b)	TA	3 µmol/kg	1 (5 m)	GEOMAR
Automatic potentiometric titrator	Hanna Instruments Titrator HI931	TA	± 4 µmol/kg	3 (6 m)	W1M3A
Automatic potentiometric titrator	Metrohm 685 Dosimat (Hernandez-Aylon, 1999)	TA	3 µmol/kg	5 (0.5, 3 m) ¹	PALOMA
Automatic potentiometric titrator	Mettler Toledo G20/SOP3b	TA	± 4 µmol/kg	10 (0.5, 2 m)	MIRAMARE
pH metre	Mettler Toledo Seven Compact	pH	± 0.001	3 (6 m)	W1M3A
Varian Cary 50 spectrophotometer	Varian, Clayton and Byrne (1993) (SOP 6b)	pH	± 0.003	5 (0.5, 3 m) ²	PALOMA
Varian Cary 100 Spectrophotometer	Varian, Clayton and Byrne (1993) (SOP 6b)	pH	± 0.002	10 (0.5, 2 m)	MIRAMARE

766 O₂=dissolved oxygen; DIC=Dissolved Inorganic Carbon; TA=Total Alkalinity.

767 ¹ For each measurement, 2 replicate samples were collected and analysed.

768 ² For each measurement, 2 replicate samples were collected and 2-3 analyses were performed at each replicate.

769 SOP=Standard Operating Procedure according to Dickson et al. (2007).

770

771 **Table S5. Temperature offsets between SD sensor (SBE37-SMP-ODO) at 0.5 m depth and fixed stations during the**
 772 **ATL2MED demonstration experiment. More details are available in Skjelvan et al. (2021).**

Fixed station/ glider	Measurement depth (m)	SD 1030 offset (°C)	SD 1053 offset (°C)
W1M3A	1	-0.006	-0.026
E2M3A	1.7	0.216	0.138
OGS ocean glider	0.5	0.063	0.063
PALOMA	0.5	0.077	0.090
PALOMA	3	-0.061	-0.046
MIRAMARE	0.5	-0.085	-0.205
MIRAMARE	2	-0.117	-0.238

773

774

775

Table S6. Overview over where to find the data used in the current work.

Platform	Variables used in current work	doi or pid	Reference
SD 1030	T, S, O ₂ , pCO ₂	https://hdl.handle.net/11676/mxGAeRL4UPrNdz08p7dBxVpR	Skjelvan and Fiedler (2024)
SD 1053	T, S, O ₂	https://hdl.handle.net/11676/4pHG8h6rGfwN_KvLSqgR1iau	Skjelvan and Fiedler (2024)
RV Meteor	T, S, DIC, TA	https://fileshare.icos-cp.eu/s/eyLp9m685QA8ME7	Paulsen et al. (2023)
RV Ucadiz	S	https://fileshare.icos-cp.eu/s/eyLp9m685QA8ME7	Gonzalez and Bruno (2024)
DYFAMED/ BOUSSOLE fixed station	T, S, DIC, TA, pCO ₂	https://doi.org/10.17882/43749	Coppola et al., 2023
Nice - Calvi glider	S	https://www.seanoe.org/data/00409/52027/ , doi from the MOOSE program (glider SLOCUM Theque on MOOSE T00_43 section)	Testor et al. (2017)
W1M3A fixed station	T, S, pCO ₂	https://hdl.handle.net/11676/Z9bGSnVObyglR0o8zcvmlXBz	Bozzano and Pensieri (2024)
E2M3A fixed station	T, S, pCO ₂	https://nodc.ogs.it/catalogs/doidetails?4&doi=10.6092/d0d50095-bd30-4ff7-8d0a-a12121e72f78	Cardin et al. (2020)
E2M3A glider	S	https://nodc.ogs.it/catalogs/doidetails?8&doi=10.13120/e7277c6b-444a-4d61-8288-596af1bac3ff	Gerin et al. (2021)
PALOMA fixed station	T, S, pH, TA, pCO ₂	https://hdl.handle.net/11676/an-PJSKTEVHj3H0gA8ak3IG	Cantoni and Luchetta (2024)

MIRAMARE fixed station	T, S, pH, TA, $p\text{CO}_2$	https://hdl.handle.net/11676/ngPlu-Q0dtDcDx2wMFTNOtnZ	Giani (2024)
Argo buoy	S	https://doi.org/10.48670/moi-00044	Wong et al. (2020)
CMEMS	Model product Chl-a SST Vertical structure of sea temperature	https://doi.org/10.25423/CMCC/MEDSEA_ANALYSISFORECAST_PHY_006_013_EAS7 ; OCEANCOLOUR_MED_BGC_L3_NRT_009_141, doi: 10.48670/moi-00297; SST_MED_SST_L4_NRT_OBSERVATIONS_010_004, doi:10.48670/moi-00172; MEDSEA_MULTIYEAR_PHY_006_004, doi:10.25423/CMCC/MEDSEA_MULTIYEAR_PHY_006_004_E3R	Clementi et al. (2021)

776 T=temperature; S=salinity; O_2 =dissolved oxygen; DIC=Dissolved Inorganic Carbon; TA=Total Alkalinity; $p\text{CO}_2$ =partial
777 pressure of carbon dioxide.
778
779
780